TEMPORAL REGISTRATION OF VESSELS IN RETINAL IMAGES

GUO XINYU

(Bachelor of Computing (Honours), NUS)

A THESIS SUBMITTED

FOR THE DEGREE OF MASTER OF SCIENCE

DEPARTMENT OF COMPUTER SCIENCE

SCHOOL OF COMPUTING

NATIONAL UNIVERSITY OF SINGAPORE

2006

Acknowledgement

During the course of this research I benefited enormously from the knowledge and expertise of my advisers, Assistant Professor Lee Mong Li, Associate Professor Wynne Hsu. I especially thank them for their patient guidance on constructing the thesis concept and many invaluable advices on my thesis progress. I also thank them for their kindness and helpfulness through the years supervising me.

Thanks to all my colleagues sitting in CHIMES lab of SoC for their moral support.

Abstract

Fundus image of human retina serves as a significant avenue for clinical doctors to monitor and probe the progress and severity of various diseases. Cardiovascular diseases such as stroke and coronary heart disease are the leading causes of morbidity and mortality worldwide and narrowing of the retinal arterioles has long been recognized as an early feature of hypertensive retinopathy and has been suggested to predict cardiovascular disease and mortality. The temporal registration of retinal images provides an important groundwork for doctors to monitor the progression of diseases. In this paper, we describe a tree matching approach to register retinal images. We model each vessel in a retinal image as a tree, called Vessel Feature Tree (VFT). We design a matching function to compute the similarity of a pair of vessels based on their VFTs. We develop a global alignment algorithm to compute the best match between the vessels in two images. Experiment results on 300 pairs of real-world retina images indicate that the proposed approach is able to achieve an accuracy of 93% and we prove that our proposed algorithm outperforms other latest developed algorithms.

Table of Contents

List of Figures

List of Tables

Chapter 1

INTRODUCTION

Image registration is the process of overlaying two or more images of the same scene taken at different times, from different viewpoints, and/or by different sensors. It geometrically aligns two images - the *Template Image* and the *Input Image*. The differences between Template Image and Input Image are introduced due to different imaging conditions and changes over time. Image registration is a crucial step in all image analysis tasks in which the final information is gained from the combination of various data sources like in image fusion, change detection, and multi-channel image restoration.

Typically, registration is required in remote sensing (multi-spectral classification, environmental monitoring, change detection, image mosaicing, weather forecasting, creating super-resolution images, integrating information into geographic information systems (GIS)), in medicine (monitoring retinal vessel changes to screen heart disease progress, treatment verification, comparison of the patient's data with anatomical atlases), in cartography (map updating), and in computer vision (target localization, automatic quality control). During the last decade, image

acquisition devices have undergone rapid development and growing amount and diversity of obtained images invoked the research on automatic image registration. In general, the applications of image registration can be divided into four main groups according to the manner of the image acquisition:

- *Different viewpoints (multi-view analysis).* Images of the same scene are acquired from different viewpoints. The aim is to gain larger a 2D view or a 3D representation of the scanned scene. Examples of applications: Remote sensing mosaicing of images of the surveyed area. Computer vision - shape recovery (shape from stereo).

- *Different times (multi-temporal analysis).* Images of the same scene are acquired at different times, often on regular basis, and possibly under different conditions. The aim is to find and evaluate changes in the scene which appeared between the consecutive image acquisitions. Examples of applications: Remote sensing - monitoring of global land usage, landscape planning. Computer vision - automatic change detection for security monitoring, motion tracking. Medical imaging - monitoring of the healing therapy, monitoring of the tumor evolution, monitoring of the vessel width change in human retinas.

- *Different sensors (multimodal analysis).* Images of the same scene are acquired by different sensors. The aim is to integrate the information obtained from different source streams to gain more complex and detailed scene representation. Examples of applications: Remote sensing - fusion of information from sensors with different characteristics like panchromatic images, offering better spatial resolution, color/multi-spectral images with

better spectral resolution, or radar images independent of cloud cover and solar illumination. Medical imaging - combination of sensors recording the anatomical body structure like magnetic resonance image (MRI), ultrasound or CT with sensors monitoring functional and metabolic body activities like positron emission tomography (PET), single photon emission computed tomography (SPECT) or magnetic resonance spectroscopy (MRS). Results can be applied, for instance, in radiotherapy and nuclear medicine.

- *Scene to model registration.* Images of a scene and a model of the scene are registered. The model can be a computer representation of the scene, for instance maps or digital elevation models (DEM) in GIS, another scene with similar content (another patient), 'average' specimen, etc. The aim is to localize the acquired image in the scene/model and/or to compare them. Examples of applications: Remote sensing - registration of aerial or satellite data into maps or other GIS layers. Computer vision - target template matching with real-time images, automatic quality inspection. Medical imaging - comparison of the patient's image with digital anatomical atlases, specimen classification.

1.1 Retinal Image Registration

Digital retinal images are widely used in the diagnosis and follow-up management of patients with eye disorders such as glaucoma, diabetic retinopathy, and age-related macular degeneration. Figure 1.1 shows a digital retinal image. Optic Disc is the circular area in the back of the inside of the eye where the optic nerve connects to the retina. Branching Point is any point in vessel where a vessel

segment splits into two children segments. Crossing Point is any point in retinal image where two vessels intersect with each other. The vascular structure of the retina plays an important role in revealing the severity of eye-related diseases. Clinical studies have suggested that the narrowing of retinal arterioles may be an early indicator of cardiovascular diseases [65]. A metric for determining the narrowing of arterioles is to compute the ratio of the diameters of arteries and veins in a digital retina image [65]. However, as diseases typically evolve over time, doctors need to monitor the changes in the diameters of vessel to determine the degree of arterioles narrowing. The first step to monitor changes in the diameters of the vessels is to register the vessels between a patient's retinal images taken at different time points.

Retinal image registration is a challenging task because it requires the accurate identification of important features in an image and an effective matching algorithm to find the correspondence of features between pair of images. This is difficult as the intensity of the retina can vary greatly and the positions of the vessels may shift. Further, the onset of diseases may also affect the vascular structure itself with vessels disappearing over time and new vessels growing. Figure 1.2 shows an example of patient's retinal images taken 5 years apart. We observe new vessels growing from a major vessel after 5 years. Figure 1.3 shows the resulting overlap image. Figure 1.4 shows another example where an existing vessel disappears. Figure 1.5 shows the resulting overlap image. These changes in the vascular structure makes registration of retinal images difficult. Vessels need to be matched to their corresponding ones between the two images, and once vessels are correctly registered, and segments of each vessel are matched, doctors are able to monitor the changes in width of vessels over time and assess the evolution of

diseases.

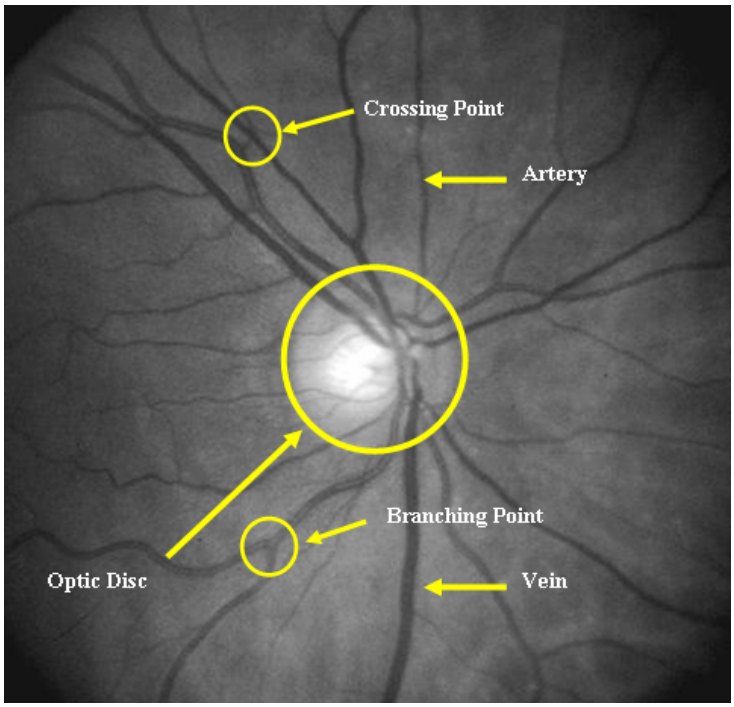

Figure 1.1: An example of a retinal image

The majority of registration methods consists of the following four steps:

- Feature detection. Salient and distinctive objects (closed-boundary regions, edges, contours, line intersections, etc.) are detected. For further processing, these features can be represented by their point representatives (line endings, distinctive points), which are called control points (CPs).

- Feature matching. In this step, the correspondence between the features detected in the Input Image and those detected in Template Image is established. Various feature descriptors and similarity measures along with spatial relationships among the features are used for that purpose.

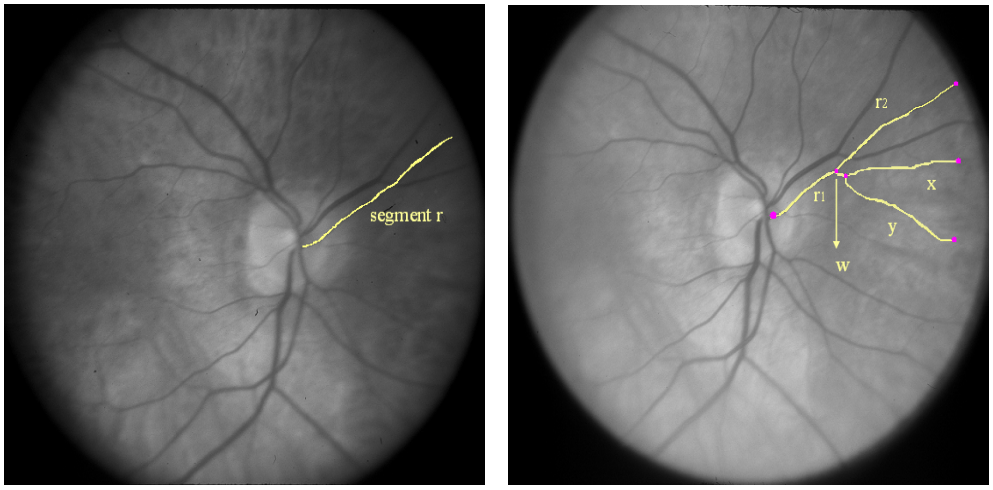

(a) Template Image (b) Input Image

Figure 1.2: (a) and (b) are retinal images of a patient's retina taken 5 years apart. Vessel segments x and y are new.

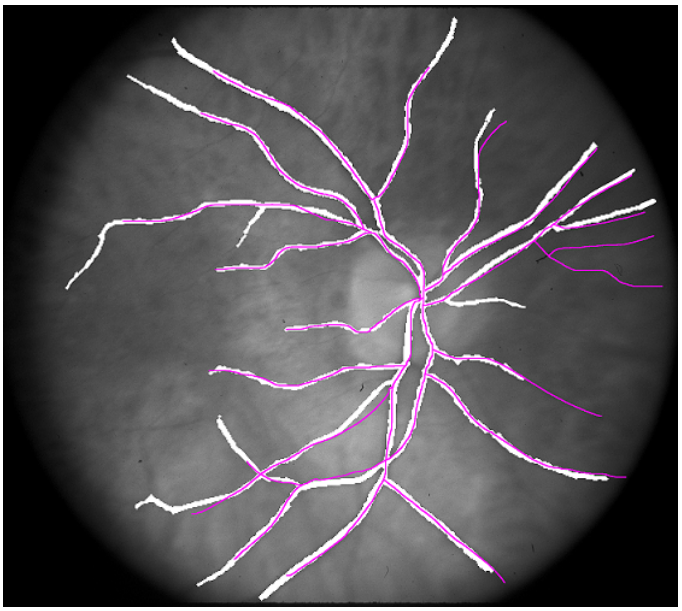

Figure 1.3: Result of registration for images in Figure 1.2, the centerline (highlighted in red) of vessels in Input Image is overlapped onto vessels (highlighted in white) in Template Image

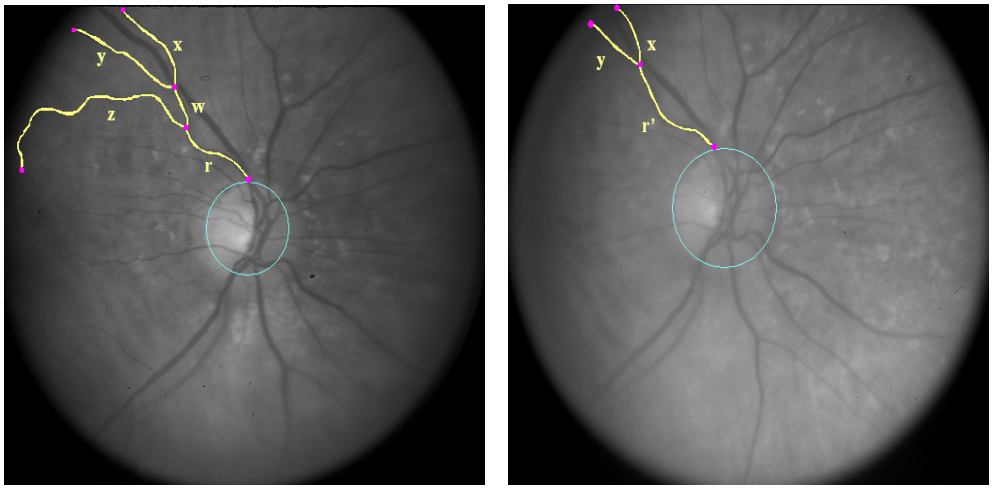

(a) Template Image (b) Input Image

Figure 1.4: (a) and (b) are retinal images of a patient's retina taken 5 years apart. Vessel segment z in (a) has disappeared in (b).

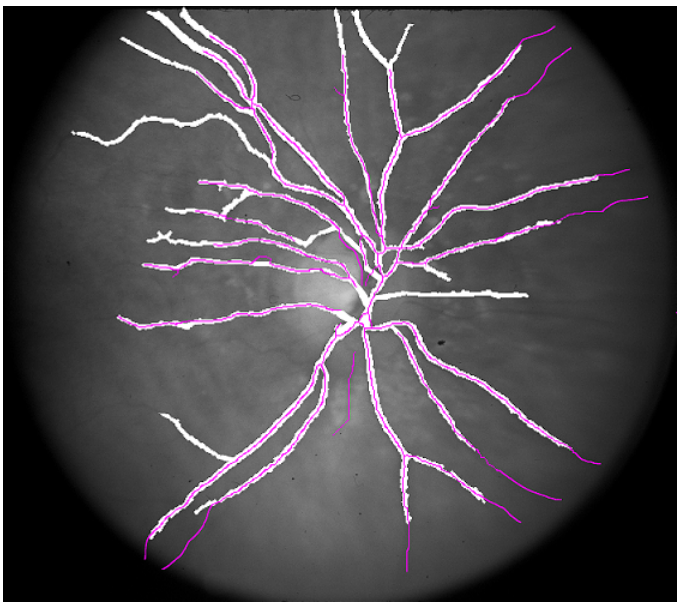

Figure 1.5: Result of registration for images in Figure 1.4, the centerline (highlighted in red) of vessels in Input Image is overlapped onto vessels (highlighted in white) in Template Image

- Transform model estimation. The type and parameters of the so-called mapping functions, aligning Input Image with Template Image are estimated. The parameters of the mapping functions are computed by means of the established feature correspondence.

- Image re-sampling and transformation. The Input Image is transformed by means of the mapping functions. Image values in non-integer coordinates are computed by the appropriate interpolation technique.

The implementation of each registration step has its problems. First, we have to decide what kind of features is appropriate for the given task. The features should be distinctive objects, which are frequently spread over the images and easily detectable. For retinal image, the usual features chosen are vascular structure and its related features, such as branching or crossing points. Usually, the physical interpretability of the features is demanded. The detected feature sets in Template Image and Input Image must have enough common elements, even in situations when the images do not cover exactly the same area or when there are object occlusions or other unexpected changes. The detection methods should have good localization accuracy and should not be sensitive to the assumed image degradation. In an ideal case, the algorithm should be able to detect the same features in all projections of the retina regardless of the particular image deformation.

In the feature matching step, problems caused by incorrect feature detection or by image degradations can arise. Physically corresponding features can be dissimilar due to the different imaging conditions and/or different spectral sensitivity of retinal camera. The choice of the feature description and similarity measure has to consider these factors. The feature descriptors should be invariant to the

assumed degradations. Simultaneously, they have to be discriminable enough to be able to distinguish among different features as well as sufficiently stable so as not to be influenced by slight unexpected feature variations and noise. The matching algorithm in the space of invariants should be robust and efficient. Single features without corresponding counterparts in the other image should not affect algorithm's performance.

The type of the mapping functions should be chosen according to the a-priori known information about the acquisition process and expected image degradations. If no a-priori information is available, the model should be flexible and general enough to handle all possible degradations which might appear. The accuracy of the feature detection method, the reliability of feature correspondence estimation, and the acceptable approximation error need to be considered too. Moreover, the decision about which differences between images have to be removed by registration has to be done. It is desirable not to remove the differences we are searching for if the aim is a change detection. This issue is very important and extremely difficult.

Finally, the choice of the appropriate type of re-sampling technique depends on the trade-off between the demanded accuracy of the interpolation and the computational complexity. The nearest-neighbor or bilinear interpolation are sufficient in most cases; however, some applications require more precise methods.

Many methods have been developed to tackle the retinal image registration problem. Generally all methods can be categorized with respect to certain criteria. We can classify registration techniques according to the similarity measures they choose in transformation model estimation step, namely intensity-based and feature-based approaches [44].

Intensity-based approaches [11] [19] [41] [31] [33] [40] [43] [48] [63] [64] use intensities or intensity gradients as similarity measures to optimize a transformation function to realize the registration. These algorithms potentially have a large number of local minimum and are expensive computationally . Moreover, intensity-based approaches are highly dependent on the consistent brightness in two images, and tend to fail if there is relatively big change in brightness between two images.

Feature-based approaches [17] [21] [23] [37] [4] [13] [7] [22] [29] [45] [49] [57] [66] align images based on correspondences between automatically detected features in two images. These approaches utilize vessel trees and branch points as similarity measure for matching. One major issue for feature-based approaches is how to successfully extract features from images and matching to consistent features. This problem is sometimes exacerbated by poor quality of image or disease progress. Besides, these features are seldom static (e.g. the appearance/disappearance of vessels), which may affect the registration accuracy.

1.2 Contributions

In this thesis, we investigate how to utilize tree matching techniques to perform retinal image registration. We first conduct a comprehensive survey over existing image registration algorithms, analyze some landmark techniques and summarize their strengths and weakness. We first describe methods to extract features from both Template Image and Input Image, including optic disc detection, vessel structure reconstruction, and we propose our own methods to track vessels and extract features such as branching point, crossing point, with, branching angles that

will be used during feature matching. Next we describe our approach to register retinal images, we model vessel tree structure as rooted trees called Vessel Feature Tree (*VFT*), thereby transforming the image registration problem into a tree matching problem. We propose a tree matching algorithm that utilizes both local and global matching functions for registration. The local matching function calculates matching cost for each pair of potential matching *VFTs*; the global matching function minimizes the global matching cost, which is the sum of matching cost for all matching pairs. The global matching function also takes into account of vessel alignments. We utilize these two functions to eventually register vessels in Template Image and Input Image. We perform a series of experiments to evaluate the performance of our registration algorithm and experiment results show that our algorithm is able to register vessels with high accuracy and robustness. From 300 randomly selected pairs of clinical retinal images, our proposed algorithm has an average accuracy of 93%. It correctly matches all the vessels in 114 pairs of images (100% accuracy), and achieves at least 90% accuracy in 75 pairs of images. 108 pairs of images achieve at least 80% accuracy. Only 3 pair of image has an accuracy below 80% due to a lesion over a large area of retinal image surface in the *Input Image*. We compare our proposed algorithm with existing algorithms [17] and [57] and show that our algorithm outperforms them.

1.3 Thesis Organization

Chapter 2 gives a comprehensive survey of existing image registration algorithms and analyze some landmark techniques. Chapter 3 presents method used in this thesis to extract features from retinal images. Chapter 4 describes transforming

retinal image registration problem into a tree matching problem, then it describes modelling each vessel structure of retinal image into a structured tree, namely Vessel Feature Tree (*VFT*) and finally presents matching functions to perform local matching and then global matching of *VFTs*. By utilizing those matching functions, we then elaborate our core algorithm to perform the registration of vessel in two images. In Chapter 5, we perform a series of experiments to evaluate the performance of our registration algorithm. In Chapter 6 makes a conclusion and identifies some possible extensions of our works.

Chapter 2

LITERATURE REVIEW

2.1 General Medical Image Registration

Medical imaging is a vital component of a large number of applications, such applications occur throughout the clinical track of events; not only within clinical diagnostics settings, but prominently so in the area of planning, consummation, and evaluation of surgical and radiotherapeutical procedures. Since information extracted from two images acquired clinically is usually of a complementary nature, proper integration of useful data obtained from the separate images is often desired. A first step in this integration process is to register those images.

Many techniques used in retinal image registrations are inspired by techniques developed for general medical image registration or for other specific medical purposes. Some of the techniques used in retinal image registration are incremental work specially designed for retinal image topologies and characteristics. Therefore, general medical image registration techniques have a huge influence on retinal image registration and are of great interest to us. In this section, we

will introduce some of the prominent general medical image registration techniques proposed to gain a better perspective of the development history of image registration. Then we will describe some techniques introduced for retinal image registration specifically.

For general medical image based registration methods, they can be generally divided into extrinsic and intrinsic. The former is based on foreign objects introduced into the imaged space, and the latter is based on the image information as generated by the patient.

2.1.1 Extrinsic Registration Methods

Extrinsic methods rely on artificial objects attached to the patient, objects which are designed to be well visible and accurately detectable in all of the pertinent modalities. As such, the registration of the acquired images is comparatively easy, fast, can usually be automated, and, since the registration parameters can often be computed explicitly, there is no need for complex optimization algorithms. The main drawbacks of extrinsic registration are the prospective character, i.e., provisions must be made in the pre-acquisition phase, and the often invasive character of the marker objects. Non-invasive markers can be used, but as a rule are less accurate.

Since extrinsic methods by definition cannot include patient related image information, the nature of the registration transformation is often restricted to be rigid (translations and rotations only). Furthermore, if they are to be used with images of low (spatial) information content such as EEG or MEG, a calibrated video image or spatial measurements are often necessary to provide spatial informa-

tion for basing the registration on. Because of the rigid-transformation constraint, and various practical considerations, use of extrinsic methods is largely limited to brain and orthopedic ([52] [14]) imaging, although markers can often be used in projective (2D) imaging of any body area. Non-rigid transformations can in some cases be obtained using markers, e.g., in studies of animal heart motion, where markers can be implanted into the cardiac wall.

2.1.2 Intrinsic registration methods

Intrinsic methods rely on patient generated image content only. Registration can be based on a limited set of identified salient points (landmarks), on the alignment of segmented binary structures (segmentation based), most commonly object surfaces, or directly onto measures computed from the image grey values (voxel property based).

Landmark based registration methods

Landmarks can be anatomical, i.e., salient and accurately locatable points of the morphology of the visible anatomy, usually identified interactively by the user ([27] [38] [34] [55] [51] [56] [61]), or geometrical, i.e., points at the locus of the optimum of some geometric property, e.g., local curvature extrema, corners, bifurcation points, etc, generally localized in an automatic fashion ([2] [60] [1] [10] [58]). Landmark based registration is versatile in the sense that it can be applied to any image. Landmark based methods are mostly used to find rigid or affine transformations. Anatomical landmarks are also often used in combination with an entirely different registration basis ([20] [34] [69] [9] [15]): methods that

rely on optimization of a parameter space that is not quasiconvex are prone to sometimes get stuck in local optima, possibly resulting in a large mismatch. A drawback is that user interaction is usually required for the identification of the landmarks.

In landmark based registration, the set of identified points is sparse compared to the original image content, which makes for relatively fast optimization procedures. Such algorithms optimize measures such as the average distance between each landmark and its closest counterpart, or iterated minimal landmark distances. For the optimization of the latter measure the Iterative closest point (ICP) algorithm [5] and derived methods are popular.

Segmentation based registration methods

Segmentation based registration methods can be rigid model based ([59] [62] [61] [69] [15]), where anatomically the same structures are extracted from both images to be registered, and used as sole input for the alignment procedure. They can also be deformable model based ([6] [3] [50] [58] [12]), where an extracted structure (also mostly surfaces, and curves) from one image is elastically deformed to fit the second image. Since the segmentation task is fairly easy to perform, and the computational complexity relatively low, the method has remained popular. Many follow-up papers aimed at automating the segmentation step, improving the optimization performance, or otherwise extending the method have been published. A drawback of segmentation based methods is that the registration accuracy is limited to the accuracy of the segmentation step. In theory, segmentation based registration is applicable to images of many areas of the body, yet in practice the application areas have largely been limited to neuro imaging, orthopedic imag-

ing and retinal imaging. The methods are commonly automated but for the segmentation step, which needs human instruction and therefore is performed semi-automatically most of the times.

With deformable models however, the optimization criterion is different: it is always locally defined and computed, and the deformation is constrained by elastic modelling constraints imposed onto the segmented curve or surface. Deformable curves appear in literature as snakes or active contours; 3D deformable models are sometimes referred to as nets. The deformation process is always done iteratively, small deformations at a time. Deformable model approaches are based on a template model that needs to be defined in one image. Opposed to registration based on extracted rigid models, which is mainly suited for intra-subject registration, deformable models are in theory very well suited for inter-subject and atlasa registration, as well as for registration of a template obtained from a patient to a mathematically defined general model of the templated anatomy. A drawback of deformable models is that they often need a good initial position in order to properly converge, which is generally realized by pre-registration of the images involved. Another disadvantage is that the local deformation of the template can be unpredictably erratic if the target structure differs sufficiently from the template structure.

Voxel property based registration methods

The voxel property based registration methods stand apart from the other intrinsic methods by the fact that they operate directly on the image grey values, without prior data reduction by the user or segmentation. There are two distinct approaches: the first is to immediately reduce the image grey value content to a

representative set of scalars and orientations, the second is to use the full image content throughout the registration process.

Voxel property based methods use full image content. Theoretically, these are the most flexible of registration methods, since they, unlike all other methods mentioned, do not start with reducing the grey valued image to relatively sparse extracted information, but use all of the available information throughout the registration process. Although voxel property based methods have been around a long time, their use in extensive 3D/3D clinical applications has been limited by the considerable computational costs.

2.2 Retinal Image Registration

Retinal image registration methods are limited to intrinsic feature based methods because it is usually impossible to implant any extrinsic object into eyes. Existing registration techniques can be categorized according to the similarity measures they choose in transformation model estimation step, namely intensity-based and feature-based approaches [44].

Intensity-based approaches [11] [19] [41] [31] [33] [40] [43] [48] [63] [64] use intensities or intensity gradients as similarity measures to optimize a transformation function to realize the registration. These algorithms potentially have a large number of local minimum and are expensive. Moreover, intensity-based approaches are highly dependent on the consistent brightness in two images, and tend to fail if there is huge change in brightness between two images.

Feature-based approaches [17] [21] [23] [37] [4] [13] [7] [22] [29] [45] [49] [57] [66] align images based on correspondences between automatically detected

features in two images. These approaches utilize vessel trees and branch points as similarity measure for matching. One major issue for feature-based approaches is how to successfully extract features from images and matching to consistent features. This problem is sometimes exacerbated by poor quality of image or disease progress. Besides, these features are seldom static (e.g. the appearance/disappearance of vessels), which may affect the registration accuracy. In this section we describe in detail some landmark registration algorithms and then analyze their performances.

2.2.1 Intensity-based Methods

Fourier Spectrum Method

Cideciyan [11] uses a multi-stage method to register retinal images. In the first stage they compute the Fourier spectrums of the two images. If the Template Image is a scaled, rotated and translated version of the Input Image then, in the Fourier spectrum, image of the Template Image will be a rotated and scaled version of the Input Image with the rotation and scaling parameters being the same with the two original images. In the second stage the log polar transformation of the Fourier spectrum images is computed, which converts the rotation and scaling differences to a translation difference. In the third stage, the rotation and scaling parameters are computed from the log-polar image pair using cross-correlation. These parameters are then used to rotate and scale one of the original images. The translation parameters can then be found via cross-correlation on the resulting pair.

Although [11] reports some good results for images taken at the same sitting,

images taken at different times may have large x translation; this would cause problems if we use the Fourier spectrum. Changes in light intensity between sittings could also cause problems with the use of cross-correlation in the second and third stage of their method.

Signal Processor Assisted Method

Wade and Fitzke [64] describe an image processing system which they develop to align autofluorescence and high-magnification images taken with a laser scanning ophthalmoscope. However, they use a modern dedicated signal processor (Matrox board) to aid their work. A window of the Template Image is matched against Input Image taking the cross-correlation as the alignment measure. They make full use of the hardware capabilities. For instance, a Gaussian filter to eliminate noise, or the full refinements of the in-box algorithmic search.

The main focus of their work is to demonstrate the capabilities of a dedicated image processing hardware for the registration of ophthalmologic images, but they do not report in detail it success for sequences other than the original images. Their algorithm runs at an average speed of 1 second on a Pentium 133MHz and the dedicated signal processor (Matrox board) configuration.

Method Using Mutual Information

Ritter [48] uses the full image content for alignment and mutual information as the similarity measure. These methods applied firstly on the registration of head images in 1995, they do not extract corresponding features but make use of all the information available. They measure the statistical dependence or information redundancy between the image intensities of pixels corresponding at both images.

In this algorithm, mutual information defined by entropy in mathematics is modified to apply for retina images to serve as the similarity calculation. Mutual information function has a natural defect, multiple local minima. In retinal image registration, some images are registered at local minima instead of at the correct global minimum. In order to tackle this problem, the algorithm adopts simulated annealing that is designed to deal with local minima and does not presuppose any particular shape for the function being searched. Further more, the algorithm institutes a system of re-annealing incorporating pyramid sampling for speed and allowing the search over fewer parameters. An interpolation is used for computing the nearest neighbor for approximation.

Although successful, the simulated annealing algorithm is highly dependent on a large number of parameters, 6 global plus 7 for each layer of the pyramidal search. These parameters are hidden deep into the code, making it impossible for a user to tune to any change in the image constraints. Their registration algorithm runs at an average speed of 3 to 38 seconds, depending on the accuracy demanded. A steep tradeoff between time and accuracy is required for their algorithm.

2.2.2 Feature-based Methods

Adaptive Adjacency Graphs

Jasiobedzki [23] suggests the use of active contours which conform to edges found by previously processing the images. These contours are active in the sense that they are controlled by an energy level that they try to minimize. This energy level is affected by the shape of the contour and surrounding image. The active contours for the Template Image are then mapped into an adaptive adjacency graph,

which is simply a network of active contours where nodes are replaced by springs that allow free movement of the contours meeting at that node. If the graph of one image is placed over another image that has the same topology of contours, then the graph will steadily move to match the Input Image, thereby successfully registering two images.

The main disadvantage of this algorithm is that the active contours are attracted only to features that they are initially close to. This means that the method would fail whenever the deformation between images is large. In temporal images it is not uncommon that x translation is as much as 70 pixels. This would make it impossible for the contours to map to the correct features in the second image.

Method Using Automatically Selected Control Point Pairs

Hart [21] utilizes control points in retinal images to perform the registration. In the proposed algorithm, a blood vessel filter [8] is applied to the green plane of an RGB image to obtain a response map, and then this map of the blood vessel filter is thinned to produce an image containing binary edge segments. The edge segments are classified afterwards to be labelled as blood vessels or non-blood vessels. Control points are identified by examining the ends of the edge segments. For every two ends of edge segments that are within 10 pixels, a single control point is extracted.

After the control points are extracted, a selection process is performed to pair each control point in the Template Image with one in the Input Image, and the next step involves removing those pairs that are more than 100 pixels apart on a coordinate system based on the estimated center of the optic nerve. A further reduction in pairs is then made by correlating the pixel intensities of a $15*15$-pixel

window centered on the control points. Erroneous pairs are now eliminated by comparing the x and y scaling factors of the pairs. Those where the two factors are quite different are discarded on the assumption that the aspect ratio between the images is unlikely to vary greatly. Pairs that are too close to previously accepted pairs are also eliminated.

A selection of the remaining pairs is then chosen and a least squares method is used to fit the current transformation to these pairs. The estimate of the transformation is then iteratively refined by removing the control point pair with the greatest error and the pair that, with its exclusion, gives the best overall error reduction. This iterative process terminates when either there are only four control points left or the mean square error drops below 5.0 pixels.

This algorithm does not work under some circumstances such as transition or rotation cases; it also cannot provide high accuracy. As it uses correlation as a measure of comparison it also has problems with temporal images that are very different in color or intensity. This is also true for images taken from patients with glaucoma. One of the signs of this disease is the loss of nerve fibers on the retina and topography of the optic disc, which can cause a significant change in pixel intensities between the two images. A further problem comes from the use of the estimated location of the optic nerve, as errors in this can affect the final registration. Blood vessels do not maintain the same position over time, this is a case where this algorithm cannot handle.

Matrices-based Method

Mendonca et al. [37] propose a matrix-based method, which involves using classical edge-detection techniques on the two images and then quantifying these data

as two matrices for each image: one recording the horizontal component of the location of edge features and the other storing the vertical component. Registration then becomes the task of aligning the two matrices to get the best fit possible, the measure of fit being calculated from the addition of the matches between the first and second pair of image matrices.

To perform the actual registration, a template area is chosen from the first pair of matrices and then matched within the pair of matrices from the second image. This is done using an exhaustive search.

While this comparison method clearly solves the problem of different intensities, it leaves two major problems unsolved: it deals only with translation, not rotation or scale changes, and it does not state clearly on how to choose the template to be matched. While the largest type of misalignment of retinal images is translation, there will be some cases where the eye is not situated at exactly the same distance from the camera, or the patient's head is tilted differently. These effects can lead to scale and rotation changes in the image data, which this algorithm can hardly handle well.

Abstract Token based Method

Pinz and coworkers [45] describe a generic method for image registration that uses tokens, which are symbolic representations based on structures extracted from the image and do not require exact correspondence to work. The algorithm defines an exponentially decreasing distance function and a hierarchical structure is built with the dilate morphological operator, which proves to be robust and suitable for a broad range of images. They also propose a method for a full mapping of the human retina. They automate detection of the vessels by the following stages: a)

extracting the edge elements along the boundary, b) grouping and search for cross sections and c) combinations of cross sections to tubes.

Their algorithm runs at an average speed of 5 to 6 minutes on a SGI O2 + KBVision hardware configuration. This time includes the full mapping of the human retina, which includes automatic detection of vessels, removal of several anatomical and pathological features: optic disc, fovea and foveola, skotoma and sub-retinal leakage.

Method Using Vessels Detection and Hough Transform

Zana [66] uses the vascular tree for bifurcation point identification. An opening with reconstruction using revolving linear structuring elements of size 15 pixels is applied to remove the noise and nonlinear parts of the image. A sum of top hats is used to enhance the contrast. Then the cross-curvature is calculated using a principal curvature evaluation. After that a simple threshold is applied on every positive value of the filtered curvature to detect vessel-like patterns. Eventually a binary image with vessel structures is obtained.

A geodesic distance is computed on the binary image of nonvascular patterns. Then a watershed is performed on the inverse of this distance image so that the vessels can be reduced to one-pixel-wide paths. Bifurcation points are detected using a supremum of openings with revolving structure elements with a T shape. And each bifurcation point is labelled with surrounding vessel orientations.

The bifurcation points may not match exactly, but during the transformation, angle between edges are preserved and bifurcation points can be identified by the directions of the branches surrounding them by means of an appropriate measure of similarity. According to the angle-based invariant, a probability is then com-

puted for points to match. Then a Bayesian Hough transform is used to sort the transformations with their respective likelihoods. A precise affine estimate is finally computed for most likely transformations. The best transformation is chosen for registration.

However, this method only utilizes individual control points and there is a high possibility that the control points are sparse and transformed so that the registration is prone to fail. Their registration algorithm runs at an average speed of 5 to 7 minutes on a Pentium 150 MHz CPU configuration.

Method Using Creases as Anatomical Landmarks

Lloret's work [29] identifies the vessel structure as an important feature for registration. Vessels are reliable landmarks in retinal images because they are almost rigid structures and they are depicted in all modalities and over time. Opposite to the bifurcation points approach, using vessel structure do not have a strong dependence of the quality of the segmentation.

They treat vessels as creases and images are seen as landscapes. They firstly start by extracting vessels by a detector of the creaseness of an image. They use a definition of crease based on level set extrinsic curvature (LSEC) and use the invariance properties for creaseness detection. They employ the MLSEC - ST operator defined in [30] for vessel extraction.

After the vessels have been extracted, they choose a cross-correlation function to match those pixels with creaseness values higher than a small fixed threshold. An iterative Simplex algorithm is developed to optimize the alignment process, a hierarchical search scheme is applied to speed up the results and add an initial wide search to improve it robustness. In their experiment they have some

appealing success rate that is lower than 5 pixels. However, they simulate the transformation on retinal images and then apply their algorithm to test the robustness. Manual simulation of transformation is not a convincing way to prove robustness; almost all the algorithms can reach an excellent success rate under manual simulation. Therefore, the effectiveness of their algorithm is still yet to be proved.

Method Using Control Points

Heneghan et al. [22] design an algorithm to register pairs of images using control points. They use two control points from each image; rigid global transform (RGT) coefficients are calculated for all possible combinations of control point pairs. The set of RGT coefficients is then exhaustively searched and the cluster of coefficients associated with the matched control point pairs is identified. This cluster is identified by calculating the Euclidean distance between each set of RGT coefficients and its Rth nearest neighbor and then using the Expectation-Maximization (EM) algorithm to identify matched pairs of control points. Once control point pairs are established, registration of the two images is achieved by using linear regression to optimize the bilinear or 2nd order polynomial.

The novelty of this approach is to use EM technique to identify the parameters of the optimal transform. EM technique is a common technique used in mathematics and datamining field for iteratively finding the maximum likelihood estimate of the parameters of a system. It has special use in cases where the data is incomplete or has missing values. They use EM technique to iteratively try matching of control points and eventually converge to certain matching.

Control points to be matched are manually selected vessel crossings, however,

in a practical situation, control points may not be easy to detect, some control points may not be detected at all if brightness condition changes dramatically over time. In the experiment they show two examples of registration. First is an example of cross-modal image registration using an optical image and a fluorescein angiogram of an eye. The second example shows an example of the registration of two images of an infant eye capture thirteen days apart. No concrete number of experiments is shown to demonstrate the accuracy or robustness of the algorithm and this algorithm is yet to prove its effectiveness.

Dual-Bootstrap Iterative Closest Point Algorithm

Stewart et al. [57] develop an algorithm for registration of retinal images, which is called ”Dual-Bootstrap Iterative Closest Point (Bootstrap ICP)”. The general idea of this approach is to start from one or more initial, low-order estimates that are only accurate in small image regions, called bootstrap regions, and expand into a globally accurate final transformation estimate. This expansion iteratively refines and extends the transformation. In each bootstrap region, the algorithm iteratively: 1) refines the transformation estimate using constraints only from within the bootstrap region; 2) expands the bootstrap region; and 3) test to see if a higher order transformation model can be used, stopping when the region expands to cover the overlap between images. Step 1) and 3), the bootstrap steps, are governed by the covariance matrix of the estimated transformation. Estimation refinement uses a novel robust version of the ICP algorithm in registering retinal image pairs, Dual-Bootstrap ICP is initialized by automatically matching individual vascular landmarks, and it aligns images based on detected blood vessel centerlines. The resulting quadratic transformations are stated to be as accurate as less than a pixel.

Stewart's algorithm has been tested over 4000 images and proven to be a very successful technique for retinal image registration. The quantitative measure of overall performance used in this paper is success rate - the percentage of image pairs for which a correct (transformation is within 1.5 pixels of the pseudo ground-truth) transformation estimate is obtained. Stewart's algorithm achieved as high as 97.0% success rate, the only few failed cases are due to having few common landmarks or a combination of sparse centerline trace points and low overlap. It is said to be able to handle lower image overlaps, image changes and poor image quality as long as there are enough common landmarks located in the image pair. Although it claims to avoid the need for expensive global search techniques, it needs to try all pairs of matches and therefore entails a long time to register pair of images. The overall time taken is approximately between 600 seconds to 1300 seconds.

However, as explained in Stewart's algorithm, ICP is based on point features; the idea of ICP is to alternate steps of: 1) closest point matching based on a transformation estimate and 2) transformation estimation based on the resulting matches until convergence to a local minimum. The initialization is crucial to ICP, and convergence and robustness to missing and misaligned structures are also important requirements. Accurate registration requires precise and repeatable estimation of image features and their intersection angles and thickness values. Besides, in the initial matching step, landmarks tend to be matched wrongly if vascular structure is dense in image pairs. The initial incorrect matching can lead ICP algorithm converging to wrong overall matching.

Elastic Matching Algorithm

Fang [17] develops two registration algorithms, a fast chamfer matching and an elastic matching applied to the vascular structure to align pairs of fundus images. The algorithm first employs a technique [16] to enhance vessels and segment them out of background by using Laplacian of Gaussian filter and morphological filters. Then the fast chamfer matching is applied to perform the registration.

The fast chamfer matching is based on an approximate Euclidean distance transformation which forms a goodness of fit objective functions. It searches for the local optimal transformation at a coarse resolution with a large number of initial positions with acceptable computation load and allow a few candidates to next finer levels for global optimal transformation search. This method is incorporated with the parametric model of rigid affine transformation. However, the fast chamfer matching suffers from problem of being trapped in the local minima; a non-parametric elastic matching method is proposed to overcome this problem.

Elastic matching first does a thinning on the binary vascular structures to obtain patterns consist of lines and curves with one pixel width. Noises are then removed and remaining lines and curves are approximated by fitting a set of straight lines which are derived by using a minimum square error procedure. Then an energy function is defined to gradually attract two patterns towards each other.

Fast chamfer has the problem of being trapped in the local minima; and the energy function defined in elastic matching uses the overall distance between two patterns to measure the deformation of one of the images. Minimizing the energy function tends to move vessels of one image towards vessels in the other image. This algorithm largely depends on the deformation of images over time. It is

highly possible for patient that dramatic deformation takes place over time, vessels cross one another and densely positioned vessels in an area. In these cases, this elastic matching fails to perform the correct registration.

2.2.3 Discussions

Intensity-based approaches have inherent disadvantage, which is they use intensities or intensity gradients as similarity measures to optimize a transformation function. They usually suffer from large number of local minima and computations are expensive. Moreover, intensity-based approaches are highly dependent on the consistent brightness in two images, and tend to fail if there is change in brightness between two images.

In feature-based approaches, methods that use control points, such as [21], [37], [66], [29], [22] and [57], are mostly used to find rigid or affine transformations. Control points are also often used in combination with an entirely different registration basis: methods that rely on optimization of a parameter space are prone to sometimes get stuck in local optima, possibly resulting in a large mismatch. A drawback is that user interaction is usually required for the identification of the control points when automated detection fails. The set of identified control points is sparse compared to the original image content, which makes for relatively fast optimization procedures. Such algorithms optimize measures such as the average distance between each landmark and its closest counterpart, or iterated minimal landmark distances. For the optimization of the latter measure the Iterative closest point (ICP) algorithm and derived methods are popular. However, this still suffers from constraint on initial step, initial step to start ICP must

be correct, or else it usually fails eventually.

Methods that extracts vessel structure from one image and elastically deform to fit the second image, such as [17] and [23], is popular since the computational complexity is relatively low. A drawback of this type of methods is that the registration accuracy is limited to the accuracy of the vessel reconstruction step. [23] used active contours as deformable curvature, the deformation process is always done iteratively, small deformations at a time. They often need a good initial position in order to properly converge, which is generally realized by pre-registration of the images involved. Another disadvantage is that the local deformation of the template can be unpredictably erratic if the target structure differs sufficiently from the template structure.

Methods using the full image content, such as Ritter, are the most flexible of registration methods theoretically, since they, unlike other methods, use all of the available information throughout the registration process. However, their use in extensive clinical registration applications has been limited by the considerable computational costs.

Chapter 3

FEATURE EXTRACTION

There is a huge number of features in the retinal image that we can extract, amongst those features we need to find appropriate ones for our temporal registration since registration requires salient features presented in both images for tree matching so that we can find the correct matching between two images. In this chapter, we first obtain the optic disc position, and then we extract features from vessels, including length, width and orientation for each vessel segment and branching angle for segments that contain branching children segments. The algorithm assumes that the input images have a resolution of 780×520, images that are of different resolution will be scaled to the expected resolution.

3.1 Optic Disc Detection

Existing optic disc detection algorithms [24] [25] [28] [35] [36] [39] [54] employ a variety of techniques to detect the optic disc, but they are neither sufficiently sensitive nor specific enough for clinical application. In this thesis we utilize a

localize-and-refine approach [42] to detect the optic disc. Briefly, we first approximate the location of the optic disc via the Daubechies wavelet transformation. The aim of wavelet transform is to ”express” an input signal as a series of coefficients of specified energy. The intensity template is employed to construct an abstract representation of the optic disc. This abstract representation of the optic disc significantly reduces the processing area, thus increasing the computational efficiency. Next, an ellipse fitting procedure is applied to detect disc contour and to filter out the difficult cases.

The result of the optic disc detection is shown in Figure 3.1.

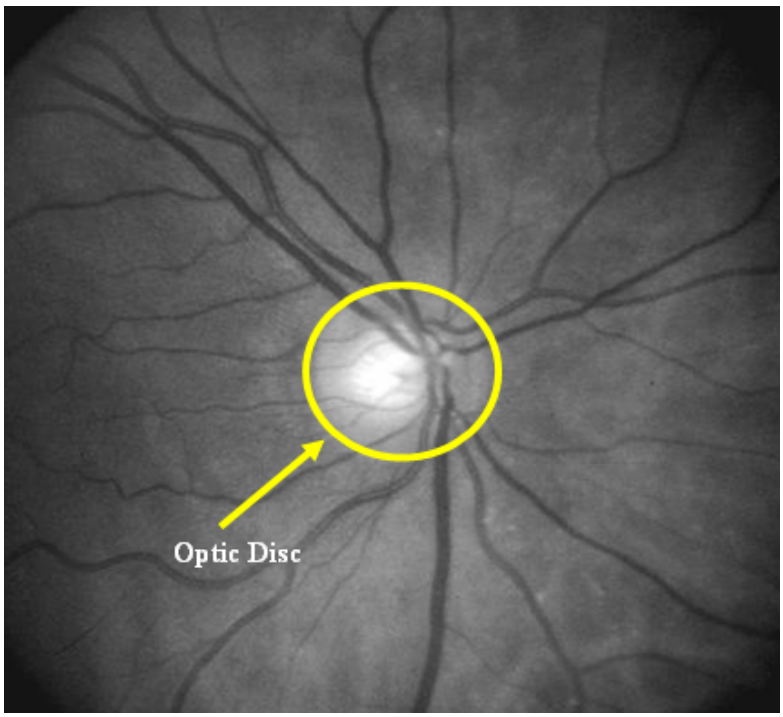

Figure 3.1: Optic disc detection result

3.2 Vessel Structure Detection

Following the detection of optic disc, we need to extract the vessel structure. Many vessel structure extraction algorithms [18] [26] [47] [67] [68] have been proposed. They typically utilize edge detectors such as Sobel, Gaussian and Laplacian of Gaussian. However, these edge detectors are not able to detect the vessel structures accurately because vessels in these retina fundus images usually have poor local contrast where the edges are rarely sharp and distinct enough to be readily identified. We implement and enhance a morphological approach to vessel structure detection [16]. It consists of three steps. 1) enhance vessels through morphological transformations; 2) a Gaussian smoothing is first performed, then the sign of Laplacian is applied to the result image of top-hats to approximate the sign of the curvature; 3) a set of filters with linear structure elements is applied to remove the enhanced noise patterns thereby producing the final images.

First step involves designing a set of linear structure elements with length equal to the maximum diameter of the primary/major vessels. We pose these elements in different orientations using a rotating angle from 0 to 180 degree. A sum of top-hats using these linear structure elements with various orientations allows us to enhance all vessels regardless of their directions, sizes, and even if they lie in the low local contrast regions.

Careful observation reveals that after enhancement, the highlighted noise tends to be weak and disorganized whose curvature oscillates between positive and negative values frequently. On the other hand, the curvature of vessels is generally of larger positive amplitudes. This gives rise to the idea of differentiating such noise from vessels by using curvature evaluation as our second step. A Gaussian

smoothing is first performed. Then the sign of Laplacian is applied to the result image of top-hats to approximate the sign of the curvature. In the third step, a set of filters with linear structure elements is applied to remove the enhanced noise patterns thereby producing the final images.

During the vessel structure detection, some branching and crossing sections of vessels will be ripped, causing vessel broken into fragments. We perform an additional operation to reconnect possibly broken branching and crossing section with the main vessels, which is caused by the filtering in the second step. On the green layer of the retinal image, we put a threshold to be 3 times of the caliber of major vessels, 36 pixels, to define the minimum length of small vessels. Any vessels whose length exceeds this threshold will be added to a list of small vessels; those with caliber below the threshold will be discarded. After we collect a list of small vessels, on both ends of the small vessel, we draw a fan sector of 90 degree radian with the direction of centerline of arc same with the slope angle as same as the small vessel at this point. We search within the fan sector area for end of other vessels. For all possible ends we have found within the sector area, we further trace to identify if it is just a short spur or a major vessel. If it is a major vessel, this small vessel has been successfully reconnected to its parent vessel; if all the ends found are short spurs, this candidate small vessel is discarded. In this way, the broken branching or crossing problem is resolved.

The result of the vessel structure extraction is a binary image as shown in Figure 3.2 where the white stripes are vessel structures.

Figure 3.2: Vessel structure detection result

3.3 Vessel Tracking

Having obtained the vessel structure, we can start tracking each vessel. We have already obtained the binary vessel structure as discussed previously, we then perform a thinning to the binary image and obtained the centerline image of all vessels. the skeleton of the vascular tree is obtained from the thinning process where pixels are eliminated from the boundaries toward the center without destroying connectivity in an eight-connected scheme [46]. The resulting centerline image is shown in Figure 3.4. Then we track each vessel along its centerline and obtain the left and right edge point in the binary image, the tracking splits at branching points and continue on its two children segments.

In the tracking process, we detect branching and crossing point (shown in Figure 3.3) and continue tracking till the end of vessel tree. To identify branching

and crossing point, we first define bifurcation point. In the 3×3 neighborhood of the centerline image, pixels with three neighbors are labelled as candidate bifurcation points. Crossing points appear in the centerline image as two bifurcation points very close to each other, we use a fixed-size circular window centered on the candidate bifurcation points, the window diameter is set equal to the largest vessel diameter expected clinically, if another bifurcation point is found within the range, the pair of points are defined as crossing points. Bifurcation points other than crossing points are defined as branching points.

At fixed interval of pixels, we take two anchor pixels (shown as red points in Figure 3.5) and draw a line that is perpendicular to the line connecting the two anchor pixels. We find a pixel on the left edge pixels that is closest to the perpendicular line, and measure the length of this diameter line. In this way, we can get diameters at the fixed interval to compute the average diameter of a vessel.

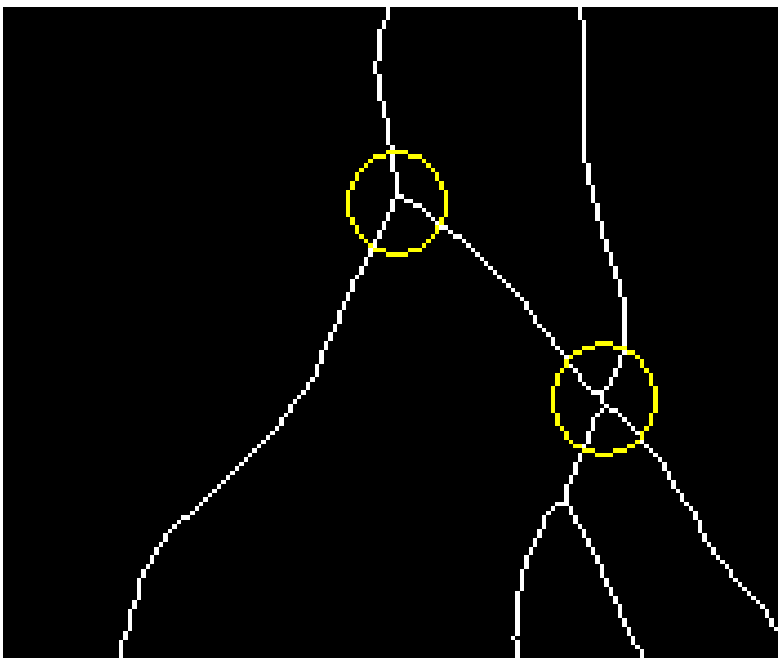

Figure 3.3: Branching and Crossing point in centerline image

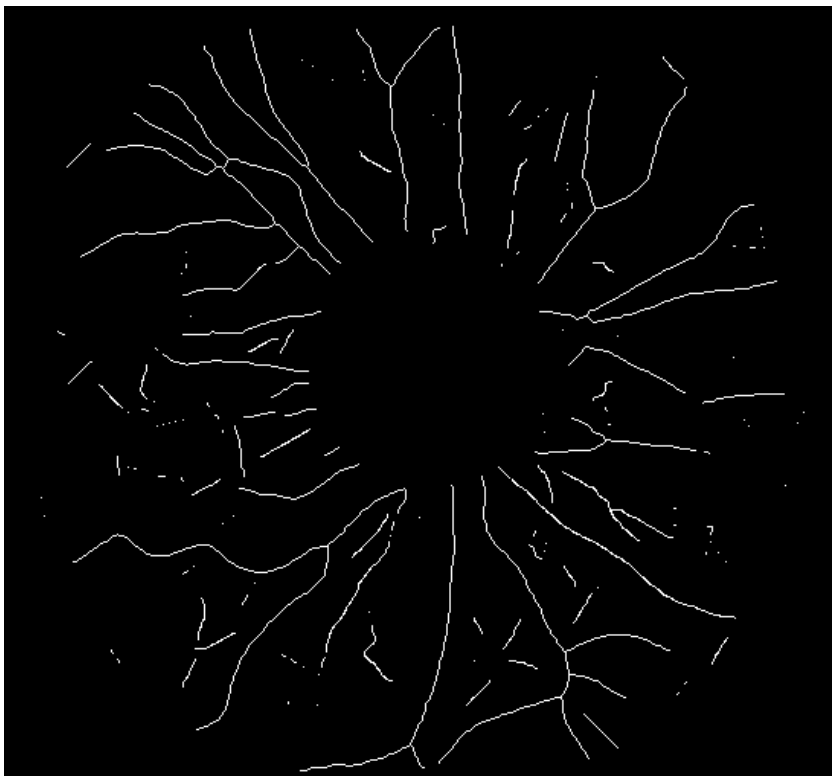

Figure 3.4: Vessel Centerline (result of thinning)

The calculation of vessel segment’s width is illustrated in Figure 3.5.

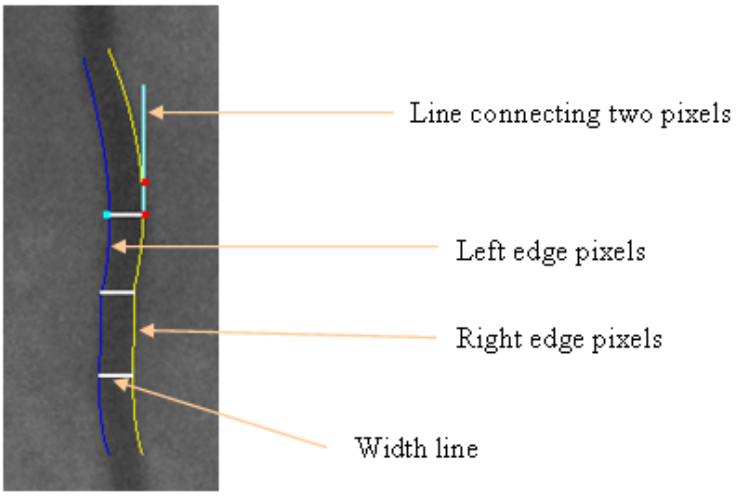

Figure 3.5: Vessel width measurement

Chapter 4

RETINAL IMAGE REGISTRATION USING TREE MATCHING TECHNIQUES

Many problems can be modelled as trees and solved using tree matching techniques. As analyzed in Chapter2, both intensity-based and feature-based algorithms suffer from their own drawbacks that affects the registration accuracy. They fail to take advantage of the entire set of available features presented in retinal images, few papers pay attention to the relationships between segments of the same vessel, such as parent and children vessel segments. The features in vessel structure are extracted while the vessel tree structure itself is left ignored; however, the structure of each vessel often contains information for registration.

Vessel trees are obvious and important structures presented in retinal images, it contains many features that can be used for registration and it does not have a strong dependence of the quality of the segmentation. In our approach, we can

utilize the overall vessel tree structures, the relationship between parent and child tree segments and transform registration problem into a tree matching problem, extract features in vessels, and model one vessel including its branches in retinal image as rooted tree and store those features in the abstract tree. Now the problem is how to measure the similarity of two trees representing two vessel structures and how to obtain the best matched ones from two retinal images.

4.1 Vessel Feature Tree

After extracting the vascular structure from a retina image. With the extracted structure, we model each vessel that originates from the optic disc as a rooted tree structure called the Vessel Feature Tree (*VFT*).

A vessel tree is divided into segments at each branch point (see Figure 4.1). A vessel tree can be mapped to a *VFT* where each node in the *VFT* corresponds to a vessel segment (see Figure 4.2). Each node is also associated with the length, diameter and branching angle of each vessel segment.

Then we make use of Vessel Feature Tree to perform registration of vessels in two images. For each image, there is a collection of *VFTs*, representing a collection of vessels in the retinal image. In our approach, we design local and global matching functions for registration. The local matching function is to calculate matching cost for each pair of potential matching *VFTs*; the global matching function is to minimize the global matching cost, which is the sum of matching cost for all matching pairs. The global matching function also takes into account of vessel alignments. Matching cost measures the goodness of *VFT* matching, a lower value means more similar two *VFTs* are. Ultimately we want to find a global matching

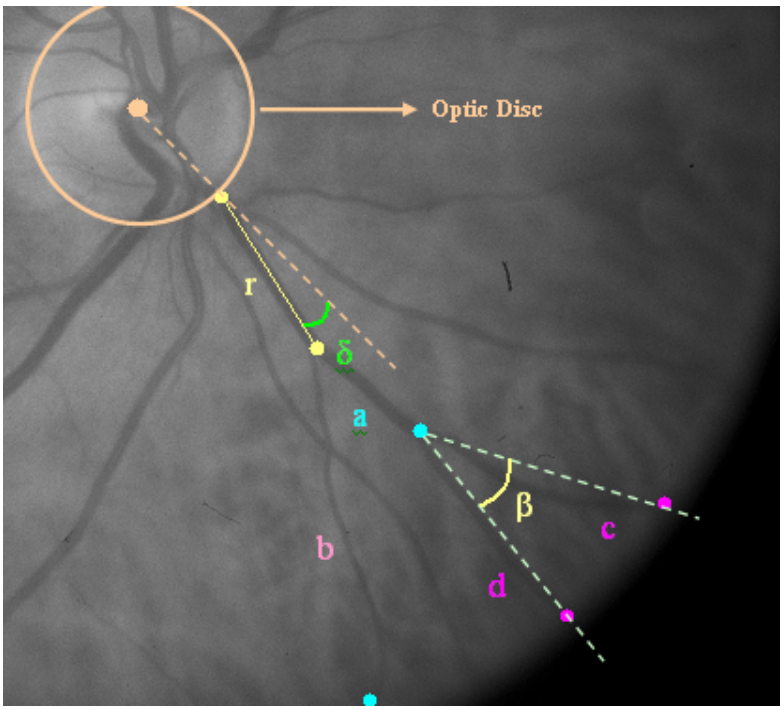

Figure 4.1: Example of a vessel tree in a retinal image. δ represents the direction angle of segment r; β represents the branching angle between segment c and d.

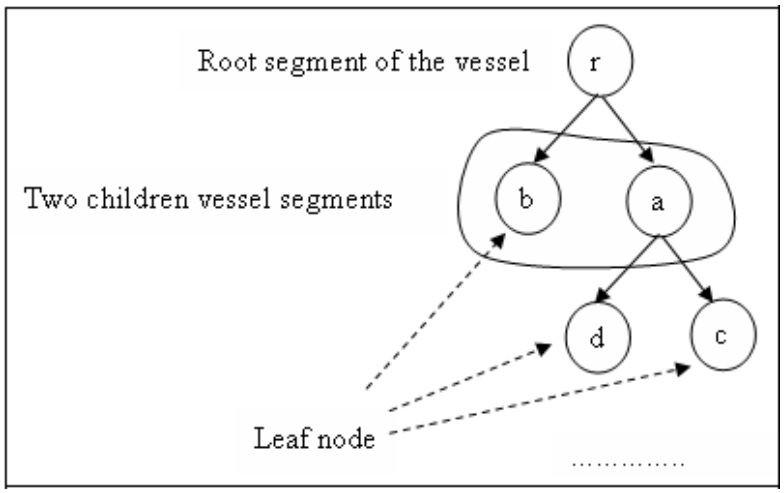

Figure 4.2: A *VFT* constructed from the vessel tree in Figure 4.1

of vessels between two images with the lowest global matching cost. We can utilize these two functions to eventually register vessels in Template Image and Input Image.

Definition: Let *VFT* = (N, E) be the Vessel Feature Tree, where N is the set of nodes and E is the set of directed edges. *VFT* is rooted, directed and acyclic. Each node *n* in N represents a vessel segment. Each edge e in E represents a branching occurs between the parent and child vessel segments. Crossing point does not create new segment, each segment remain as a single segment after the crossing point.

The root node in the *VFT* represents the vessel segment starting from the optic disc. *VFT* is a strict binary tree, each segment has 0 or 2 children due to the bifurcation property of vessels [32]. Figure 4.2 shows the *VFT* constructed from the vessel tree in Figure 4.1. Segments r, a, b, c and d in the vessel tree in Figure 4.1 are represented by nodes r, a, b, c and d in Figure 4.2 respectively.

Each node n in a *VFT* has three attributes: length, width and direction, represented by $n.L, n.W$ and $n.\delta$ respectively. The length attribute stores the length of the vessel segment along its centerline from its start to its end point. The width attribute stores the average width of the segment. The direction attribute captures the angle between the segment's centerline, and the line formed by the optic disc and the segment's start point (see angle δ in Figure 4.1). We also store the depth of a node from its root, denoted by $n.\lambda$. Further, each internal node in a *VFT* has an additional attribute called the branching angle, denoted by $n.\beta$. The branching angle of a segment measures the angle between two child segments (see angle β in Figure 4.1).

With the *VFT*, we are able to know if there is a growth of new vessel segments or if an existing vessel segment has disappeared. We design matching function to compute the similarity of two vessel trees, and transform the original registration problem into finding the optimal match of *VFTs* between two retinal images. This ensures that the registration algorithm is robust to handle any deformation in the retinal images. The features computed from previous chapter are shown in Figure 4.1.

4.2 Matching Vessel Feature Trees

For each image, we will have a set of *VFTs*, representing a collection of vessels in the retinal image. Now we need to find matching pair of *VFTs* in two images. We design local and global matching functions to achieve this. The local matching function calculates the matching cost for each pair of potential matching *VFTs* while the global matching function minimizes the global matching cost, which is the sum of matching cost for all matching pairs. The global matching function also takes into account vessel alignments. Matching cost measures the goodness of *VFT* matching, a lower value means more similar two *VFTs* are. Ultimately we want to find a global matching of vessels between two images with the lowest global matching cost. We can utilize these two functions to eventually register vessels in Template Image and Input Image.

Matched *VFTs* do not necessarily have the same number of nodes or levels, because a segment of vessel is missed during detection or a false detected segment presents in either of the *Template Image* and the *Input Image*. The complication prompts us not to pursue exact matching of trees. In exact matching, two trees are

matched if they have the same number of nodes and at each level in the tree their nodes are perfectly matched. Instead, we seek for the best approximate matching of two trees. However, we do impose penalties for mismatched nodes at each level, the cost for mismatch of nodes should increase sub-linearly. In order to correctly compute the matching cost of two *VFTs*, we need to address the following issues:

- The same vessel in two images does not necessarily have the same number of segments. This may be due to the growth of a new vessel or failure to detect a vessel segment in one of the images.

  For example, in Figure 1.2(a), the highlighted vessel has only one segment *r*. However, in Figure 1.2(b), several new segments have grown from this vessel. Segment *r* in Figure 1.2(b) is now split into segments r_1 and r_2. Our matching algorithm should match *r* to r_1 and r_2, and impose penalties for segments without any matches, i.e. *w*, *x* and *y*.

- A vessel segment might disappear over time due to the progression of disease or eye movement rotation. This causes the deletion of the node representing this segment in *VFT*. If this node has a sibling, we need to combine the sibling with its parent node.

  For example, segments *r*, *w*, *x*, *y* and *z* are five segments in a vessel in Figure 1.4(a). However, segment *z* has disappeared in Figure 1.4(b). Therefore, in the corresponding *VFT*s (see Figure 4.3), we need to delete the node *z* that represents segment *z* in Figure 1.4(a), and match nodes *r* and *w* in VFT_1 to node *r'* in VFT_2. Nodes *x* and *y* in VFT_1 are matched to nodes *x* and *y* in VFT_2 respectively.

- Finally due to scaling problem, we need to formulate the cost function with respect to the relative differences of angle, width and length between two nodes in *VFT* instead of matching the exact value.

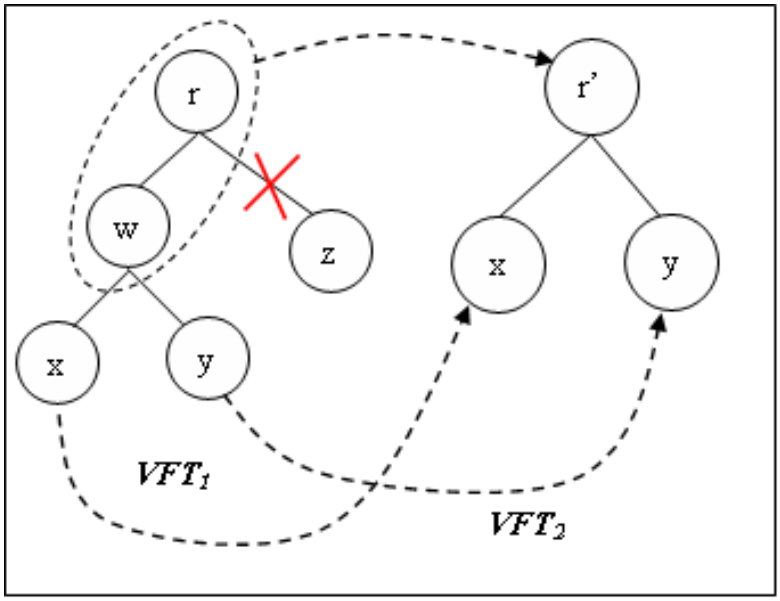

Figure 4.3: Two *VFTs* constructed from the highlighted vessel trees in Figure 1.4. VFT_1 represents the vessel in Figure 1.4(a), VFT_2 represents the vessel in Figure 1.4(b)

4.2.1 Vessel Matching Functions

For the *Template Image*, we have $S_1 = VFT_1, VFT_2, \ldots, VFT_n$, *n VFTs*, each VFT_i in S_1 represents a vessel in the *Template Image*. For the *Input Image*, we have $S_2 = VFT_1, VFT_2, \ldots, VFT_m$, *m VFTs*, each VFT_j in S_2 represents a vessel in the *Input Image*. *n* is not necessarily equal to *m*. S_1 and S_2 are the collections of all *VFTs* in the *Template Image* and the *Input Image* respectively. For the problem of registering vessels in retinal images, for each VFT_i in S_1, we

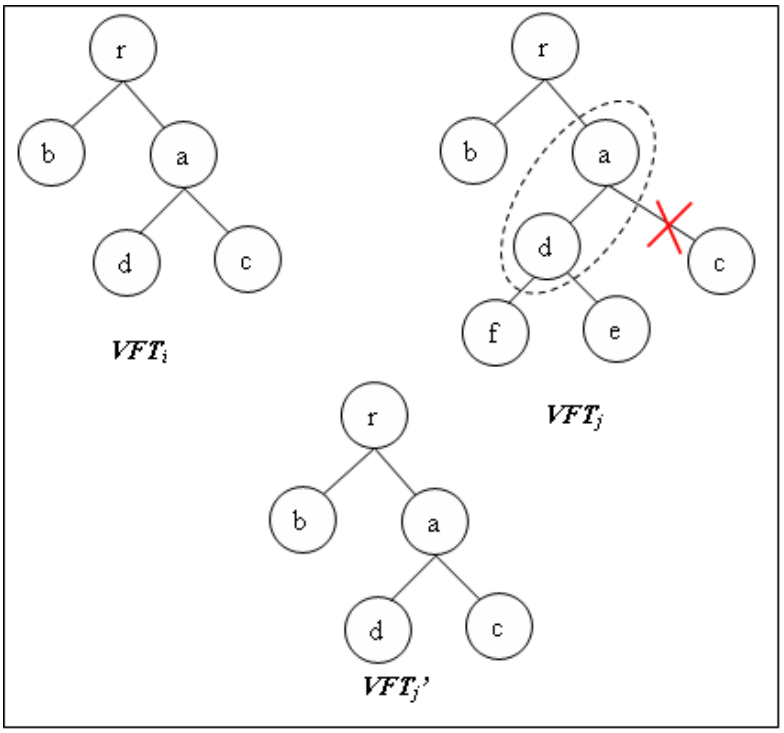

Figure 4.4: Example of matching concept

want to find a correspondence in S_2. Of course not all *VFTs* in S_1 can find its matching in S_2 due to reasons that we have mentioned above. In our algorithm, we perform two matching, local and global matching.

We measure the goodness of matching by comparing the similarity of attributes' values in *VFTs'* nodes instead of *VFTs'* structural similarity. An example is illustrated in Figure 4.4. In this example, VFT_i represents a vessel tree in *Template Image*, VFT_j represents the same vessel tree in *Input Image* as VFT_i does in *Template Image*; however, a new small vessel segment branches out from segment a in *Input Image*, causing node *a* in VFT_i to split into two nodes *a* and *d* in VFT_j, node *c* represents the newly grown vessel segment. Now node *a* in VFT_i represents a vessel segment that is represented by the combination of node *a* and node *d* in VFT_j. $VFT_j{}'$ represents a completely different vessel tree in *Input Image* and attributes in each node differ hugely from attributes in nodes of VFT_i. By only looking at the structure of these three *VFTs*, $VFT_j{}'$ is a more suitable match with VFT_i; however, the length, width or direction attributes of each node in VFT_i differ hugely with attributes of matched node in $VFT_j{}'$. Instead, attributes of nodes in VFT_i and VFT_j have close values, implying similar vessel structure in images. In this case, VFT_j are preferred by VFT_i over $VFT_j{}'$ even though the structure of $VFT_j{}'$ is more similar to VFT_i.

In this thesis, we look for matching of *VFTs* with similarity carried by feature attributes stored in each VFT nodes instead of similarity of rigid *VFT* structure. To achieve this, we need to adopt a more flexible matching manner of *VFTs*. In the example shown in Figure 1.2, node a in VFT_i corresponds to combined path a and d in VFT_j, attributes of the combined path are highly similar with node a in VFT_i. In this case, we can match node *a* in VFT_i to the merged node $\{a, d\}$ in

VFT_j; in the meantime we need to delete node *c* as it is a superfluous node and impose a cost on this deletion. We refer this match as multiple segment match, we will define a match function later to handle this case.

4.2.2 TreeMatch Function

We define a *TreeMatch* function to compute the cost of matching two *VFTs*. *TreeMatch* calls the functions *SingleSegmentMatch* and *MultiSegmentMatch*.

Given two *VFT* VFT_1 and VFT_2, the *SingleSegmentMatch* function computes the matching cost between a node n_i in VFT_1 and a node n_j in VFT_2. Two nodes are similar if their vessel lengths, average vessel widths and branching angles are similar. The three factors are incorporated into the formula below:

$$SingleSegmentMatch(n_i, n_j) = \frac{1}{\sqrt{\lambda}}(|n_i.L - n_j.L| + k_1 \times |n_i.W - \sigma \times n_j.W| + k_2 \times |n_i.D - n_j.D| + k_3 \times |n_i.A - n_j.A|) \quad (1)$$

where λ is the maximum of the depths of nodes n_i and n_j (the root is at depth 1); σ is the degree of vessel width narrowing between children and parent vessel segment[1]; k_1, k_2 and k_3 are the normalizing for width, direction and branching angle respectively. In our experiment, we set $k_1 = MaxL \times \frac{1}{MaxW}$, $k_2 = MaxL \times (1 + \sqrt{\frac{n_i L}{MaxL}})$, $k_3 = MaxL \times (1 + \sqrt{\frac{n_i L}{MaxL}})$ where MaxL and MaxW are the upper bounds for the length and width attributes respectively.

As mentioned, a new vessel may cause single segment to split into multiple segments. Hence it is crucial to compute the matching cost between a node and a path (multiple segments). The formula for matching a node n_i to multiple segments denoted by a path p_j match is as follows:

[1]the value of σ is obtained through experiments.

$$MultiSegmentMatch(n_i, p_j) = \frac{1}{\sqrt{\lambda}}(|n_i.L - p_jL| + k_1 \times |n_i.W - \sigma \times p_j.W| + k_2 \times |n_i.D - p_j.D| + k_3 \times |n_i.A - p_j.A|) \quad (2)$$

where

$$p_j.L = \sum_{n_j \in p_j} n_j.L$$

$p_j.W$ is the average width of vessel segments on p_j; $p_j.D$ is the direction of p_j calculated by connecting the start point of first node and the end point of the last node on p_j; and $p_j.A$ is the last branching angle along the path p_j.

The *TreeMatch* algorithm will utilize the two functions described above to compute the total matching cost for a pair of *VFTs*.

Algorithm 1 TreeMatch Algorithm

Input: n_i, root node of VFT_i and n_j, root node of VFT_j
Output: matching cost of VFT_i and VFT_j.
Cost1$\leftarrow$ 0;
Cost2$\leftarrow$ 0;
if (both n_i and n_j are leaf nodes) **then**
  return $SingleSegmentMatch(n_i, n_j)$;
end if
if (n_i is nonleaf node and n_j is leaf node) **then**
  return $SingleSegmentMatch(n_i, n_j)$+ $Penalty(n_i)$;
end if
if (n_j is nonleaf node) **then**
  Cost1=$SingleSegmentMatch(n_i, n_j)$;
  if (n_i is nonleaf node) **then**
    Cost1+=$TreeMatch(left(n_i), left(n_j))$+ $TreeMatch(right(n_i), right(n_j))$;
  end if
  $p_j \leftarrow SelectSegments(n_i, n_j)$;
  Cost2=$MultiSegmentMatch(n_i, p_j)$;
  if (n_i is nonleaf node) **then**
    Cost2+=$TreeMatch(left(n_i), left(p_j))$+ $TreeMatch(right(n_i), right(p_j))$+ $DeletionCost(p_j)$;
  end if
end if
return $min\{Cost1, Cost2\}$;

$left(n_i)$ and $right(n_i)$ represent the left and right child of node n_i respectively. Starting from the root nodes of the two *VFTs*, we consider both SingleSegmentMatch and MultipleSegmentMatch and select the match that gives the lowest cost. This procedure terminates when we reach the leaves of both *VFTs*. Finally, we pick the lowest matching cost as the final cost to match the two *VFTs*.

$Penalty(n_i)$ computes the penalty imposed on this matching because the subtree of n_i fails to match to any node in VFT_j and it is defined as follows:

$Penalty(n_i) = \frac{1}{2\times\sqrt{\lambda}} \sum_{n_j \in subtree\ of\ n_i} (n_i.L + k_1 \times n_i.W + k_2 \times n_i.D + k_3 \times n_i.A)$ (3)

where the symbols have the same interpretations as in SingleSegmentMatch.

The $SelectSegments$ function selects the path p_j to be matched in MultipleSegmentMatch. Essentially, it adopts a greedy approach to pick a series of segments that minimizes the overall matching cost. For example, in Figure 1.2, as nodes r_1 and r_2 in the *Input Image* represent node r in the *Template Image*, the combined segments by r_1 and r_2 have the most similar attributes value with segment r and *MultiSegmentMatch* function yields the lowest cost. Therefore, $SelectSegments$ selects segments r_1 and r_2 to be matched. Once the segments are selected, we need to delete those unwanted siblings (segments w, x and y) of the selected segments. For this, we impose a deletion cost on this deletion. The $DeletionCost$ function is defined as follows:

$DeletionCost(p_j) = \frac{1}{2\times\sqrt{\lambda}} \sum_{n_j \in siblings\ of\ nodes\ in\ p_j} (n_j.L + k_1 \times n_j.W + k_2 \times n_j.D + k_3 \times n_j.A)$ (4)

4.3 Registration of Images

In this section, we describe how the Vessel Feature Trees can be utilized to find the corresponding vessels between two images, hence registering the images. We observe that the starting points of major vessels are unlikely to shift such that one vessel crosses over another one within optic disc boundary over time.

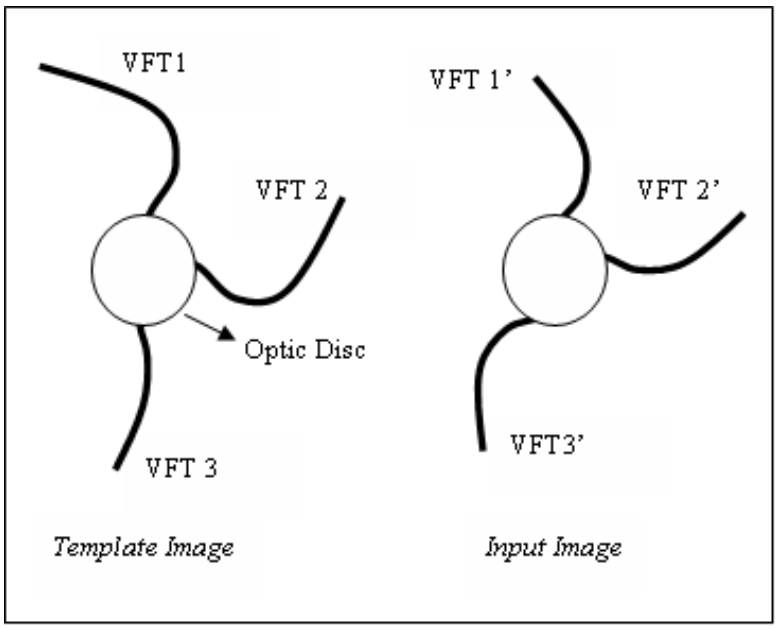

Figure 4.5: Example of vessels alignment

We can globally align *VFTs* in both images clockwise according to their start points (see Figure 4.5). During registration, we approximate the position of the matching VFT_j in *Input Image* for VFT_i in *Template Image*. Based on the *VFTs* that have already been paired up, if j goes too far from the previous matched position m in *Input Image*, this j may be a wrong match. Therefore we can utilize this observation to prune incorrect matching.

We have $S_1 = \{v_1, v_2, \ldots, v_n\}$, *n VFTs*, each v_i represents a vessel tree in

Template Image; and $S_2 = \{w_1, w_2, \ldots, w_m\}$, *m VFTs*, each w_i represents a vessel tree in *Input Image*. S_1 and S_2 are the collections of all *VFTs* in *Template Image* and *Input Image* respectively. *n* is not necessarily equal to *m*. Our goal is to find a mapping from S_1 to S_2 with minimum total matching cost. We also need to take into account of global vessel alignment described by the observation mentioned earlier. As we do not allow multiple *VFTs* from S_1 to map to the same *VFT* in S_2, if $n < m$, every v_i are matched to a distinct w_j; else, only *m VFTs* in S_1 are matched to *m* distinct *VFTs* in S_2.

Our registration algorithm has two main steps:

Local Matching Stage: For each $v_i \in S_1$, we compute the matching cost for each pair of (v_i, w_j) by $TreeMatch(v_i, w_j)$ where $w_j \in S_2$. At the end of this stage, each v_i maintains its preference list of *VFTs* in S_2 ordered by ascending matching cost; the most preferred w_j for each v_i gives the lowest matching cost. Each w_j also maintains its preference list of *VFTs* in S_1 ordered by ascending matching cost. A *CostMatrix* maintains the pairwise matching cost for each pair of (v_i, w_j).

Global Alignment Stage: We compute the optimal matching from S_1 to S_2 taking alignment of *VFTs* according to the observation described earlier into consideration. For a $v_i \in S_1$, take (v_i, w_j) such that w_j is its most preferred *VFT*; use this pair as anchor pair to reorganize S_1 and S_2 to S_1' and S_2' respectively. $S_1' = \{v_1', v_2', \ldots, v_n'\}$ where v_1' is v_i in anchor pair and rest of *VFTs* in S_1' are ordered clockwise starting from v_1'. $S_2' = \{w_1', w_2', \ldots, w_m'\}$ where w_1' is w_j in anchor pair and rest of *VFTs* in S_2' are ordered clockwise from w_1' according to their start points. $R_v[i]$ is the preference list for v_i' in S_1', $R_w[j]$ is the preference list for w_j' in S_2', $M_v[i]$ is the matching *VFT* for v_i' and $M_w[j]$ is the matching *VFT* for w_j'.

We then compute an optimal matching from S_1' and S_2' with **algorithm 2** and its corresponding cost.

This stage is iterated until all $v_i \in S_1$ and its corresponding most preferred *VFT* is used as anchor pair to reorganize S_1 and S_2 and compute an optimal matching. Finally the optimal matching with the lowest cost are selected and we thereby register vessel trees to their correspondence between two images.

In Figure 4.5, suppose the most preferred nodes for *VFT1*, *VFT2* and *VFT3* are *VFT1'*, *VFT3'* and *VFT2'* respectively. We first start by fixing the pair (*VFT1*, *VFT1'*) and rematch rest of *VFTs* clockwise, whereby *VFT2* and *VFT3* are mapped to *VFT2'* and *VFT3'* respectively. Because each pairs has similar topology and attribute values, this global matching yields a very low cost. Then we fix the pair (*VFT2*, *VFT3'*) and rematch the rest *VFTs*, VFT1 and VFT3 are matched to VFT2 and VFT1 respectively. Clearly this is not an optimal matching and cost is higher than the first matching, we thereby prune this matching. Same procedure are done for the pair (VFT3, VFT2') and finally we obtain the optimal matching and its corresponding cost. The final matching is (*VFT1*, *VFT1'*), (*VFT2*, *VFT2'*) and (*VFT3*, *VFT3'*).

Algorithm 2 describes the case when $n \leq m$, if $n > m$, the direction of matching can be simply reversed. We formulate global vessel alignment as *AlignCost* function that computes the realignment cost. *Reorganize* function simply reposition w in $R_v[v]$ according to $w's$ new matching cost,c. *AlignCost* function is defined as follows:

$$AlignCost(i, v, M_v) =$$

$$\frac{1}{\sqrt{n}}(\sum_{\forall m \in [i,v)} CostMatrix(m, M_v[m]))$$

where $n = |i - v|$

With the Local Matching and Global Alignment Stage, we match vessels from Template Image to their corresponding ones in Input Image. At the end of registration each vessel in Template Image has one and only one distinct corresponding vessel in Input Image and registration is thus achieved.

Algorithm 2 Algorithm to compute optimal matching

Input: R_v, R_w and *CostMatrix*
Output: A global matching of *VFTs* between S'_1 and S'_2.
Cost$\leftarrow$ 0;
for $i \in \{1, n\}$ **do**
  $M_v[i] \leftarrow$ free, rejected[i]$\leftarrow$ 0, $M_w[i] \leftarrow free$;
end for
$v \in \{1, n\}$, $w \in \{1, m\}$;
while v is not matched yet **do**
  $w \leftarrow R_v[v]$[rejected[v]+1];
  if ($M_w[w]$ = free) **then**
    if ($\forall i < v$, $M_v[i] < w$) **then**
      $M_v[v] \leftarrow w$, $M_w[w] \leftarrow v$;
      $Cost \leftarrow Cost + CostMatrix(v, w)$;
    else
      $c \leftarrow CostMatrix(v, w) + AlignCost(i, v, M_v)$;
      $R'_v[v] \leftarrow$Reorganize($R_v[v], c, w$);
      if ($w = R'_v[v]$[rejected[v]+1]) **then**
        $M_v[v] \leftarrow w$, $M_w[w] \leftarrow v$;
        $Cost \leftarrow Cost + CostMatrix(v, w)$;
      else
        rejected[v]$\leftarrow$ rejected[v]+1;
      end if
    end if
  else
    $v' \leftarrow M_w[w]$;
    if (RANK($R_w[w], v$)<RANK($R_w[w], v'$)) **then**
      if ($\forall i < v$,$M_v[i] < w$) **then**
        rejected[v']$\leftarrow$ rejected[v']+1;
        $M_v[v'] \leftarrow$free,$M_v[v] \leftarrow w$,$M_w[w] \leftarrow v$;
        $Cost \leftarrow Cost - CostMatrix(v', w) + CostMatrix(v, w)$;
      else
        $c \leftarrow CostMatrix(v, w) + AlignCost(i, v, M_v)$;
        $R'_w[w] \leftarrow$ Reorganize($R_w[w], c, v$);
        if (RANK($R'_w[w], v$)<RANK($R'_w[w], v'$)) **then**
          rejected[v']$\leftarrow$rejected[v']+1;
          $M_v[v'] \leftarrow$ free, $M_v[v] \leftarrow w$, $M_w[w] \leftarrow v$;
          $Cost \leftarrow Cost - CostMatrix(v', w) + CostMatrix(v, w)$;
        else
          rejected[v]$\leftarrow$ rejected[v]+1;
        end if
      end if
    else
      rejected[v]$\leftarrow$ rejected[v]+1;
    end if
  end if
end while
return M and Cost;

Chapter 5

Experiment Study

In this section, we present the results of our experiments to evaluate the performance of our proposed approach. Then we compare our proposed algorithm with other two latest registration algorithms, [17] and [57]. The results demonstrate that our algorithm is able to register vessels in temporal images with excellent accuracy, it is also highly reliable and robust under different circumstances. Besides, our algorithm yields better results compared to other algorithms, puts more focus on vascular structures and captures missing and newly grown vessel structure, which enables doctors to better evaluate disease progress after registration process.

5.1 Experiment Setup

In our experiment, we use the Blue Mountain Eye Study images that are 5 years apart. The Blue Mountain Eye Study is a population-based follow-up study of vision and common eye diseases, hearing loss and other health outcomes in an

urban population aged 49 years or older. 3654 Baseline participants represented 82.4% of eligible potential participants living in two postcode areas of the Blue Mountains region, west of Sydney, Australia. The baseline survey (1992 - 1994) methods and procedures have been previously described [65]. At the examinations, stereoscopic retinal photographs of the macula, optic disc and other retinal fields of both eyes were taken, using a Zeiss FF3 fundus camera (Carl Zeiss, Oberkochen, Germany). The data sets are purely collected by ophthalmologists and all of the images are raw data without reconciliation. The data set contains retinal image of both healthy and pathologic participants, and therefore includes all kinds of complications in images, such as brightness changes, rotation, transformation, missing vessels, etc. This data set serves as a much stronger and convincing set for both accuracy and robustness test.

A random selected sample of 300 pairs of right eye photographs was used. The selection is purely random and no conditions are imposed. We conducted a number of experiments to assess the accuracy and robustness of our registration algorithm. Vessels in our experiment image data set have more significant variations and pose greater challenges for our algorithm.

5.2 Accuracy Study

We evaluate the accuracy of our algorithm by computing the percentage of vessels that have been successfully matched in each pair of images. A pair of vessels is considered to be successfully matched if these two vessels indeed represent the same vessel in a patient's retina.

Suppose n vessels are detected in the first image (or *Template Image*), and m

vessels are detected in the next consecutive image (or *Input Image*). Then

$$accuracy = x/min(n, m)$$

where x is the number of pairs of correctly matched vessels.

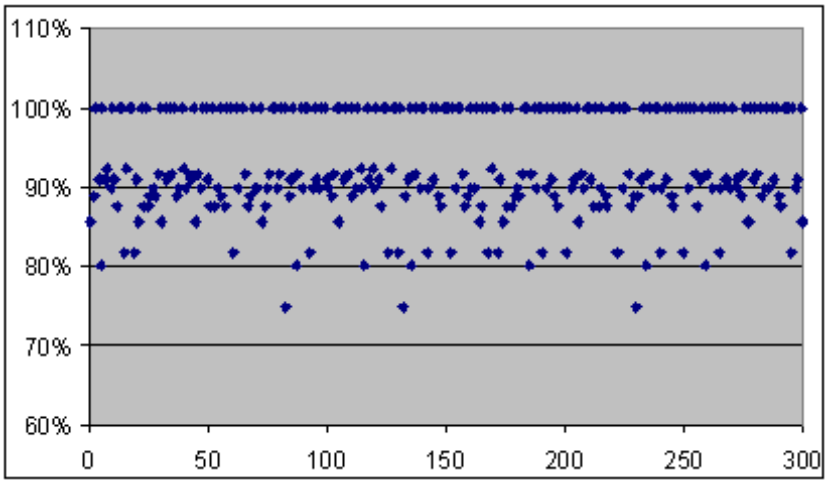

Figure 5.1: Results of accuracy experiment on 300 pairs of retina image. X axis represents the success rate. Y axis represents number of images

Figure 5.1 and Figure 5.2 show that the registration algorithm has an average accuracy of 93%. It correctly matches all the vessels in 114 pairs of images (100% accuracy), and achieves at least 90% accuracy in 75 pairs of images. 108 pairs of images achieve at least 80% accuracy. Only 3 pair of image has an accuracy below 80% due to a lesion over a large area of retinal image surface in the *Input Image*. Table 5.1 summarizes the average statistics in the accuracy experiment.

Figures 5.3, 5.4 and 5.5 show examples of successful registration even when vessels appear or disappear in the Input Image and have poor image quality with large area of bright regions. Figure 5.6 shows an example of unsuccessful registration due to failure in the vessel extraction process.

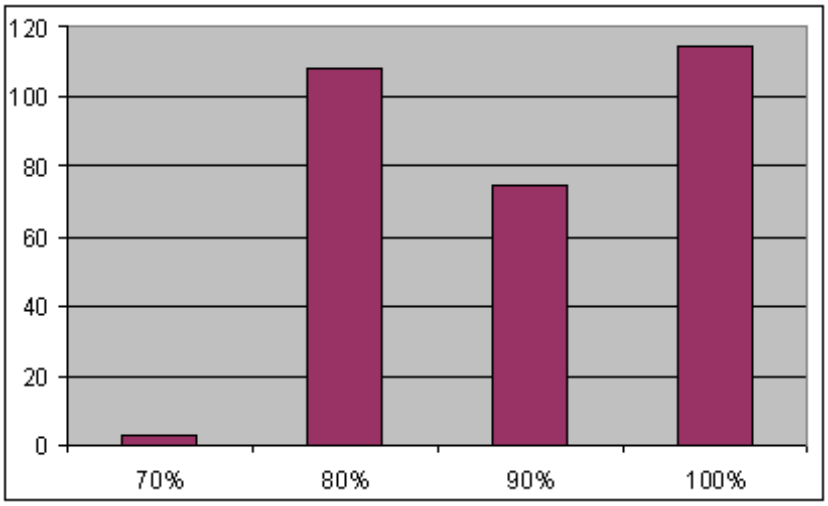

Figure 5.2: Results of accuracy experiment on 300 pairs of retina image. X axis represents the number of images. Y axis represents number of success rate. 70% indicates images with success rate less than 80%, 80% contains the images with success rate between 80% and 90%, 90% contains the images with success rate between 90% and 100% and 100% contains the images with success rate to be 100%

Average Number of Vessels	Average Number of Matches	Average Number of Mismatches	Success Rate
9.64	8.95	0.69	93%

Table 5.1: Summary of average accuracy experiment statistics. 9.64 vessels are detected in each image on average. Out of the 9.64 vessels, an average of 8.95 pairs of vessels are registered correctly, 0.69 vessels are matched to wrong vessels or without a match. The average registration success rate is 93%.

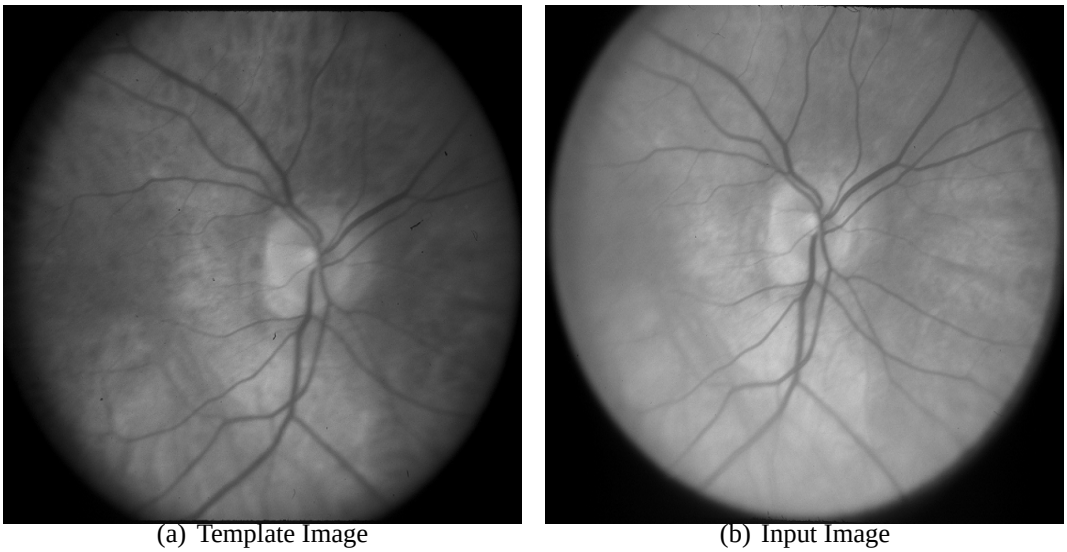

(a) Template Image (b) Input Image

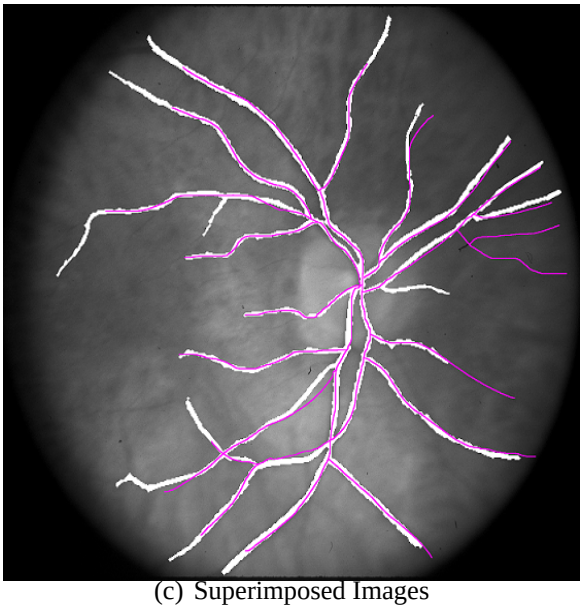

(c) Superimposed Images

Figure 5.3: Successful registration results I. Images have newly grown vessels over time

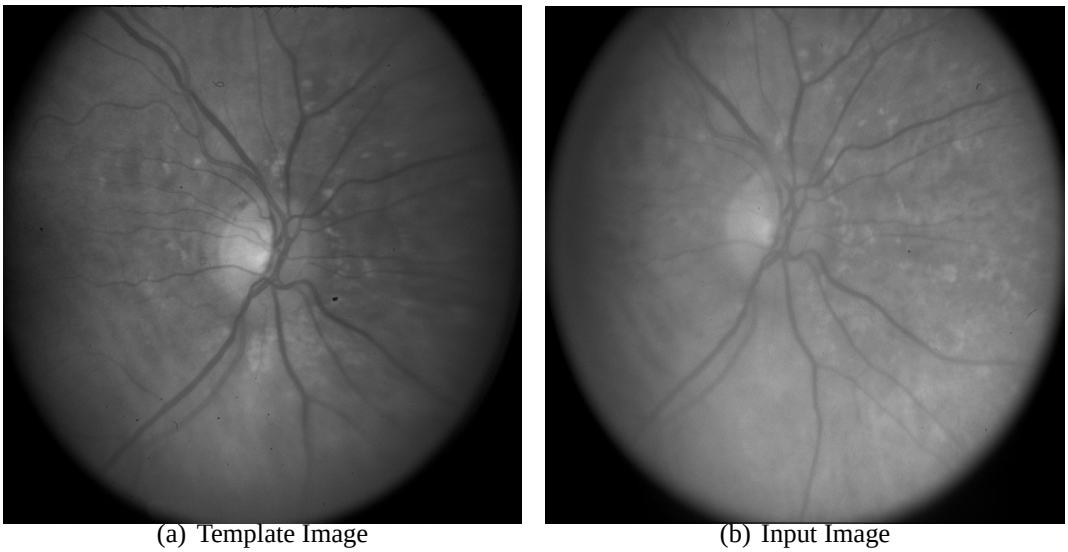

(a) Template Image (b) Input Image

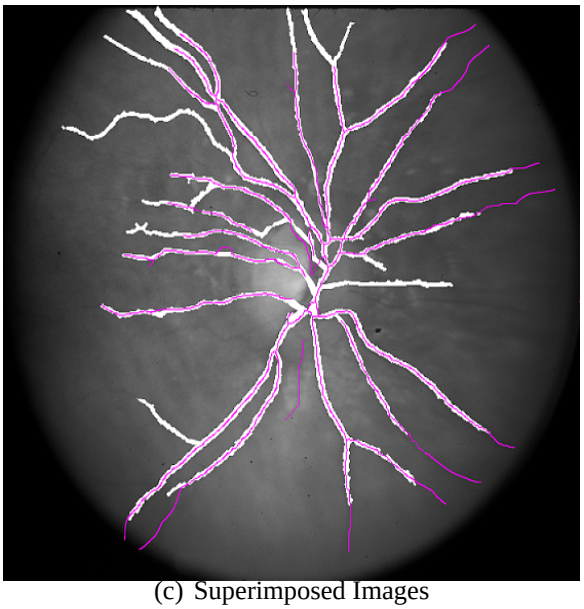

(c) Superimposed Images

Figure 5.4: Successful registration results II. Images have disappearing vessels over time

(a) Template Image (b) Input Image

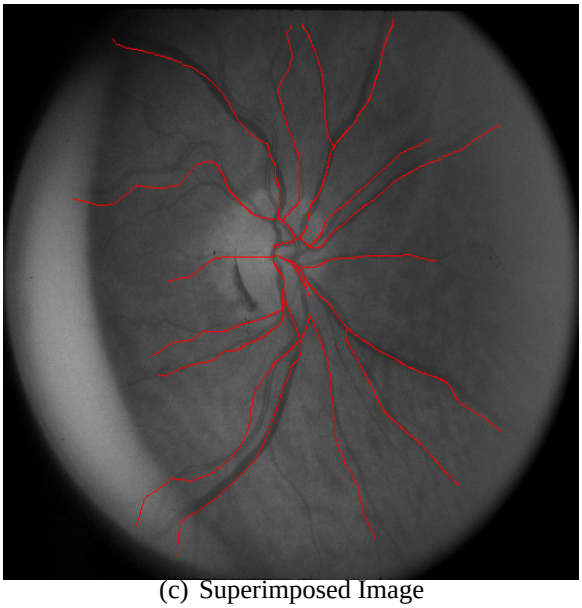

(c) Superimposed Image

Figure 5.5: Successful registration results III. Images have large area of abnormally bright region

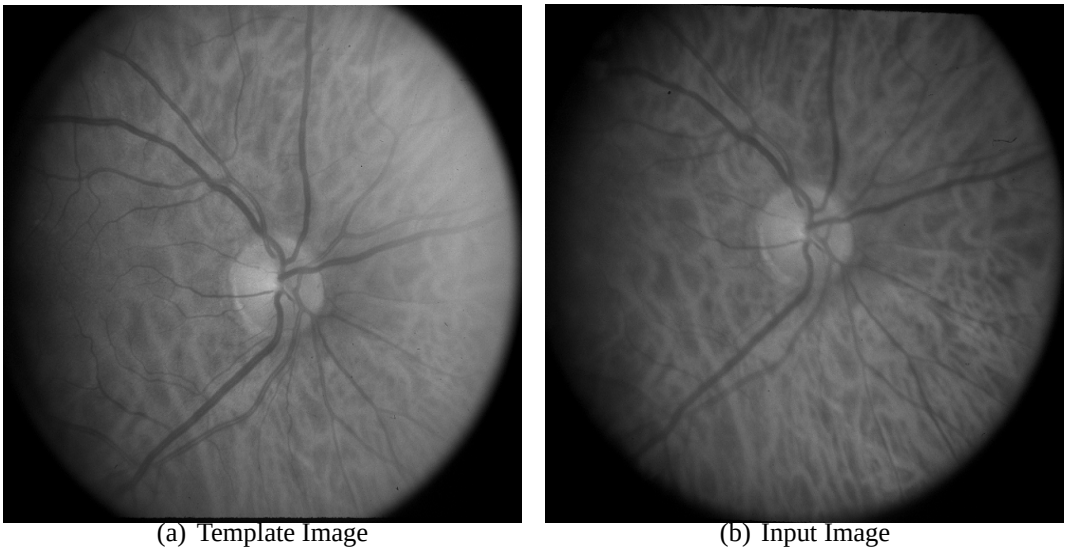

(a) Template Image (b) Input Image

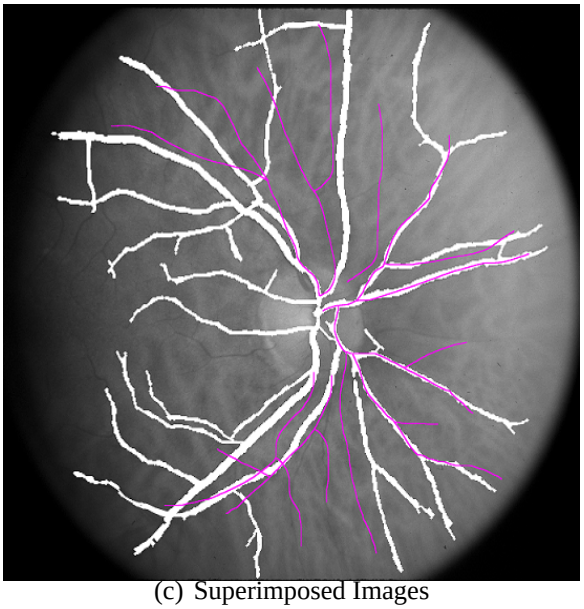

(c) Superimposed Images

Figure 5.6: Unsuccessful registration results. Images have bad quality and blurry vessels

5.3 Comparative Study

In this section we compared our proposed algorithm with the elastic matching in [17] and Dual-Bootstrap approach in [57].

We re-implemented [17] so that its accuracy can be assessed using our *Success Rate*. Its accuracy is also measured by the Success Rate defined above in Accuracy Experiment section. We obtained executable file of [57] from its authors.

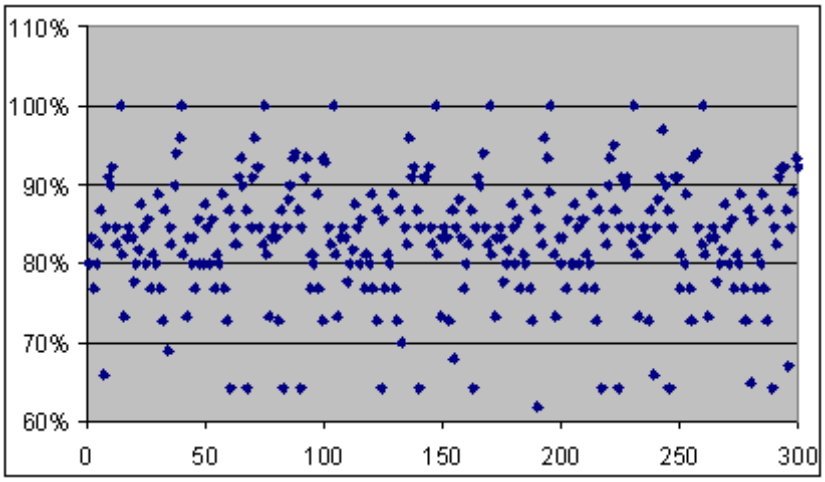

Figure 5.7: Results of accuracy experiment on 300 pairs of retina image for [17]. X axis represents the success rate. Y axis represents number of images

Average Number of Vessels	Average Number of Matches	Average Number of Mismatches	Success Rate
9.64	8.01	1.63	83%

Table 5.2: Summary of average accuracy experiment statistics for [17]. 9.64 vessels are detected in each image on average. Out of the 9.64 vessels, an average of 8.01 pairs of vessels are registered correctly, 1.63 vessels are matched to wrong vessels or without a match. The average registration success rate is 83%.

Figure 5.7 and Figure 5.8 show that [17] has an average accuracy of 83%. Table 5.2 summarizes the average statistics in the accuracy experiment. From the

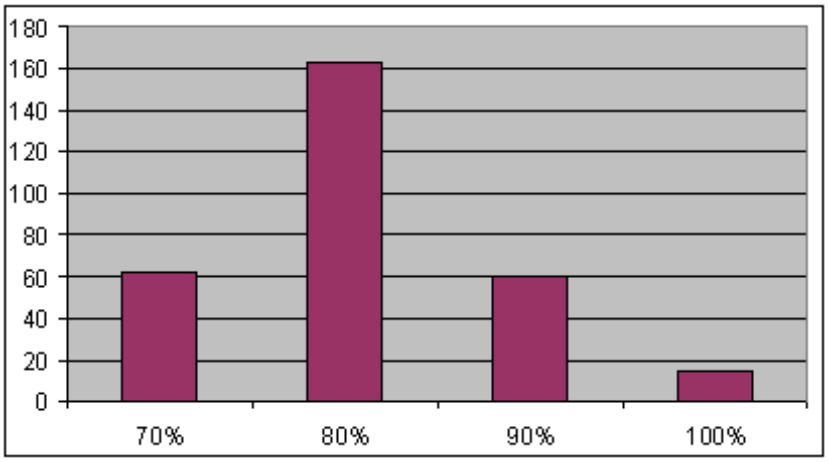

Figure 5.8: Results of accuracy experiment on 300 pairs of retina image for [17]. X axis represents the number of images. Y axis represents number of success rate. 70% indicates images with success rate less than 80%, 80% contains the images with success rate between 80% and 90%, 90% contains the images with success rate between 90% and 100% and 100% contains the images with success rate to be 100%

experiment results we can see that our proposed algorithm yields a more accurate result than [17].

For [57], the quantitative measure of overall performance is the percentage of image pairs for which a correct (transformation is within 1.5 pixels) transformation estimate is obtained. The result yields a 96% accuracy running on 300 pairs of images for [17]. Figure 5.9 shows an example of successfully registered images by [57]. The failed cases are due to having bright region in the images. Figure 5.10 shows the Template and Input image that [57] fails to register, however our proposed algorithm is able to handle this case and the superimposed image is shown previously. We modify our algorithm to conform to [57]'s metrics, with threshold set at 1.5 pixels, our algorithm has a slightly lower accuracy, which is 92%.

For processing time, our proposed algorithm takes on average 80.3 seconds to complete the whole registration process; [17] takes on average 240.4 seconds

to complete and [57] takes 1154.3 seconds to complete. This shows our algorithm takes much shorter time to process and outperforms both [17] and [57] in processing time aspect.

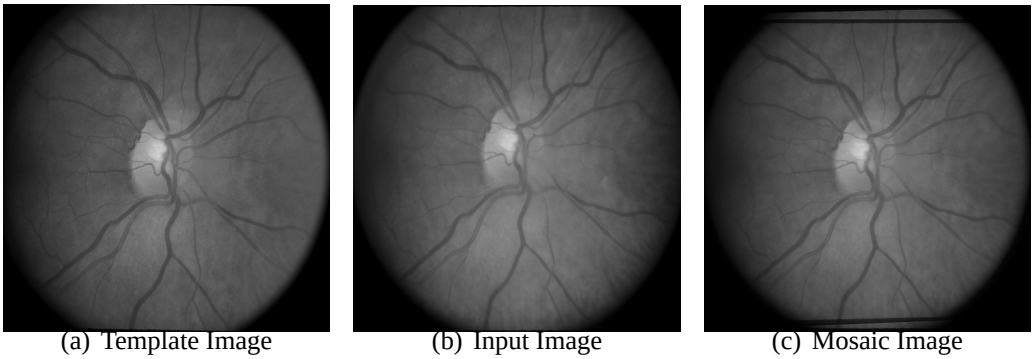

(a) Template Image (b) Input Image (c) Mosaic Image

Figure 5.9: Successful case for [57].

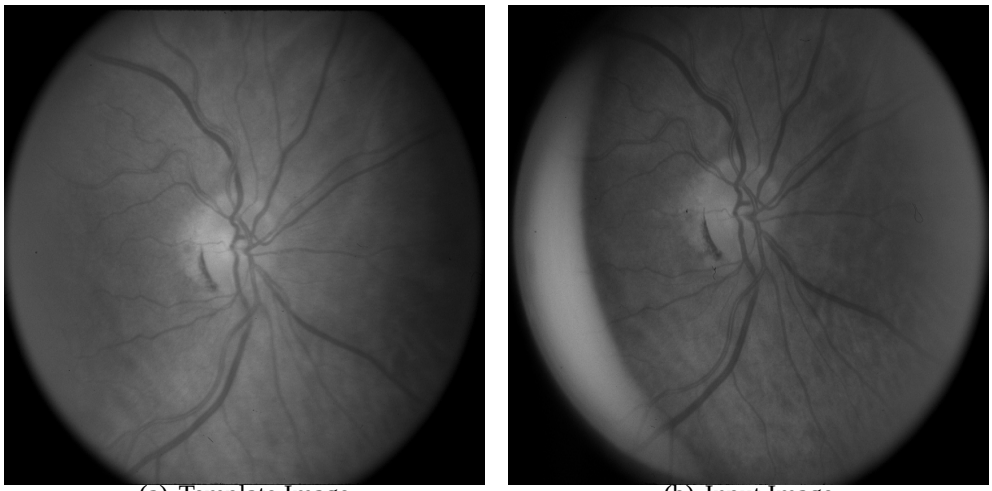

(a) Template Image (b) Input Image

Figure 5.10: Failed case for [57].

5.4 Discussions

We have introduced our proposed algorithm, which utilizes vessel trees as abstract structures and formulate the problem as tree matching problem to achieve registration purpose. This approach is different from many other existing registration approaches. In comparison to existing retina image registration approaches, it handles image changes, poor image quality, inconsistency of image brightness, missing and newly grown vessel structures. Our proposed algorithm captures the vessel trees in retina images well and use them as key features for registration. Our algorithm performs registration from a global view and gain higher accuracy, in the meantime, it also captures missing or newly grown vessel structures during registration and facilitate future analysis.

We compared our proposed algorithm with two latest existing algorithms, [57] and [17]. The experiment results show that our algorithm achieves a higher accuracy compared with [17] but slightly lower accuracy compared with [57].

The advantage of our algorithm is that we are able to capture the structure of missing vessel structures and branches, in the monitoring process doctors are able to utilize these information to better evaluate the disease development. The failed cases for Stewart's algorithm are due to having a large bright region in the image, however, our algorithm is able to handle this kind of cases well. For those cases that [57] failed to register correctly, our algorithm is able to achieve excellent registration results. Our algorithm's performance is superior than [17] in most cases, and is superior than [57] under circumstances that vessel trees are the focus in registration. This is because our algorithm is able to capture various features for vessel trees and register them with excellent accuracy. Besides our algorithm

is able to handle bright regions in retina images.

Chapter 6

Conclusion

In this thesis, we firstly investigated the importance of retinal image registration, we also did a comprehensive survey over various types of registration techniques and performed analysis of several landmark techniques. As analyzed in section 2, for intensity-based algorithms, they all suffer from a major drawback which is dependence on consistent brightness in two images. If there is huge brightness change between two images caused either by exposure of photographs or disease development, algorithms pertaining to this category can hardly yield convincing results. For existing feature-based algorithms, each algorithm utilizes one extracted feature, such as centerline, tangent direction, width, branching and cross-over points, from retinal image to perform the registration. This causes problems during registration or even failures if the quality of Input Image is poor, over exposure of photographs so that some features are missing in Input Image, etc. They fail to take advantage of the entire set of available features presented in retinal images, few papers pay attention to the relationships between segments of the same vessel, such as parental segment and children branches. The pieces of features in

vessel structure are extracted while the structure itself is left ignored; however, the structure of each vessel often contains information for registration.

In our proposed algorithm, We avoid the problems encountered by existing techniques, make use of all available features presented in retinal images and model vessel structures as rooted trees, namely Vessel Feature Trees (*VFT*), each segment of vessel is represented by a tree node, a branching of vessel into two children vessels are represented by edge and children nodes in *VFT*. By modelling vessel structures in retinal images as *VFTs*, we transform the original registration problem into tree matching problem; our target is to find a matching in Input Image for each *VFT* in *Template Image* whereby global matching cost is minimized. We use vessel features, vessel segment length, width, orientation and branching angle, as similarity measures in matching function.

We proposed a local matching function to calculate matching cost for each pair of potential matching vessels and a global matching function to minimize the global matching cost, taking into account of vessel alignments and eventually register vessels in Template Image and Input Image.

Experiment results show that our algorithm is able to match vessels in retinal image with excellent accuracy. Our algorithm is able to achieve an average success rate of 93%. For the isolated registration algorithm, the median processing time is 2.21 seconds. Worst case performance is 3.38 seconds.

The registration algorithm proposed in this paper is not only accurate, but also efficient. This algorithm can be applied in clinical retinal disease diagnosis and provides the fundamental groundwork for further medical research.

6.1 Future Work

Retinal images registration has vast range of applications. It is merely the first step towards curing some of the most fatal diseases in the world; there are plenty of works to be done. In this paper, we described a novel registration technique for registering vessels in temporal retinal images. This algorithm successfully registers detected vessels from Template Image to Input Image. From this point, we can extend our work to detect the change in AVR and changes of widths in individual vessels. This enables us to assess the impact of disease development on patients.

Also, to further make use of the parent and child branch structure provided by our algorithm, we can monitor the disappearance of some small vessels or discovering newly grown small vessels, this provides crucial information and keeps doctors on alert for some cardiovascular diseases [53].

After we successfully register two images, in our *VFT* structure, we already store the orientation of each vessel segment, we can advance our research in gauging the tortuosity changes of each vessels over time.

Bibliography

[1] Y. Amit and A. Kong. Graphical templates for model registration. *IEEE Transactions on pattern analysis and machine intelligence*, 18:225–236, 1996.

[2] T. Ault and M. W. Siegel. Frameless patient registration using ultrasonic imaging: a preliminary study. *Journal of image guided surgery*, 1:94–102, 1995.

[3] E. Bainville, G. Champledoux, P. Cinquin, V. Dessenne, A. Hamadeh, J. Troccaz, S. Lavallee, O. Peria, P. Sautot, and R. Szeliski. Anatomical surfaces based 3d/3d and 3d/2d registration for computer assisted medical interventions. *Computer vision, virtual reality, and robotics in medicine*, 19:53–65, 1995.

[4] D. E. Becker, A. Can, H. L. Tanenbaum, J. N. Turner, and B. Roysam. Image processing algorithms for retinal montage synthesis, mapping, and realtime location determination. *IEEE Trans. Biomed. Eng.*, 45:105–118, 1998.

[5] P. J. Besl and N. D. McKay. A method for registration of 3-d shapes. *IEEE Transactions on pattern analysis and machine intelligence*, 14:239–256, 1992.

[6] M. Bro-nielsen. Modelling elasticity in solids using active cubes c application to simulated operations. *Computer vision, virtual reality, and robotics in medicine*, 905:535–541, 1995.

[7] A. Can, C. V. Stewart, B. Roysam, and H. L. Tanenbaum. A feature-based, robust, hierarchical algorithm for registering pairs of images of the curved human retina.

IEEE Trans. Pattern Anal. Machine Intell., 24:347–364, 2002.

[8] S. Chaudhuri, S. Chatterjee, N. Katz, M. Nelson, and M. Goldbaum. Detection of blood vessels in retinal images using two-dimensional matched filters. *IEEE Trans. Med. Image.*, 8:263–269, 1989.

[9] G. E. Christensen, A. A. Kane, J. L. Marsh, and M. W. Vannier. Synthesis of an individual cranial atlas with dysmorphic shape. *IEEE computer society press*, pages 309–318, 1996.

[10] C. S. Chua and R. Jarvis. 3d free-form surface registration and object recognition. *International journal of computer vision*, 17:77–99, 1996.

[11] A. V. Cideciyan, S. G. Jacobson, C. M. Kemp, R. W. Knighton, and J. H. Nagel. Registration of high resolution images of the retina. *Proc. SPIE: Medical Imaging VI: Image Processing*, 1652:310–322, 1992.

[12] C. Davatzikos and J. L. Prince. Brain image registration based on curve mapping. *IEEE workshop on biomedical image analysis*, pages 245–254, 1994.

[13] B. Ege, T. Dahl, T. Sndergaard, O. Larsen, T. Bek, and O. Hejlesen. Automatic registration of ocular fundus images. *Workshop on Computer Assisted fundus Image Analysis*, 2000.

[14] R. E. Ellis, S. Toksvig-Larsen, M. Marcacci, D. Caramella, and M. Fadda. A biocompatible fiducial marker for evaluating the accuracy of ct image registration. *Computer assisted radiology*, 1124:693–698, 1996.

[15] A. C. Evans, S. Marrett, J. Torrescorzo, S. Ku, and L. Collins. Mri-pet correlation in three dimensions using a volume of interest (voi) atlas. *Journal of cerebral blood flow and metabolism*, 11:69–78, 1991.

[16] B. Fang, W. Hsu, and M. Lee. Reconstruction of vascular structures in retinal images. *IEEE International Conference On Image Processing*, 2:157–160, 2003.

[17] B. Fang, W. Hsu, and M. Lee. Techniques for temporal registration of retinal images. *IEEE International Conference On Image Processing*, 2004.

[18] L. Gang, O. Chutatape, and S. M. Krishnan. Detection and measurement of retinal vessels in fundus images using amplitude modified second-order gaussian filter. *IEEE Transactions on Biomedical Engineering*, 49:168–172, 2002.

[19] J. V. Hajnal, D. L. G. Hill, and D. J. Hawkes. Medical image registration. *FL: CRC*, 2001.

[20] A. Hamadeh, P. Sautot, S. Lavallee, and P. Cinquin. Towards automatic registration between ct and x-ray images: cooperation between 3d/2d registration and 2d edge detection. *Medical robotics and computer assisted surgery*, pages 39–46, 1995.

[21] W. E. Hart and M. H. Goldbaum. Registering retinal images using automatically selected control points pairs. *IEEE International Conference on Image Processing*, 1994.

[22] C. Heneghan, P. Maguire, N. Ryan, and P. D. Chazel. Retinal image registration using control points. *IEEE International Symposium on Biomedical Imaging*, pages 349–352, 2002.

[23] P. Jasiobedzki. Registration of retinal images using adaptive adjacency graphs. *6th IEEE Symposium Computer-Based Medical Systems*, pages 40–45, 1993.

[24] M. Lalonde, M. Beaulieu, and L. Gagnon. Fast and robust optic disc detection using pyramidal decomposition and hausdorff-based template matching. *IEEE Transactions on Medical Imaging*, 2001.

[25] S. Lee and M. Brady. Optic disc boundary detection. *British Machine Vision Conference*, 1989.

[26] T. Lei, J. K. Udupa, P. K. Saha, and D. Odhner. Artery-vein separation via mra - an image processing approach. *IEEE Transactions on Medical Imaging*, 20:689–703,

2001.

[27] W. D. Leslie, A. Borys, D. McDonald, J. O. Dupont, and A. E. Peterdy. External reference markers for the correction of head rotation in brain single-photon emission tomography. *European journal of nuclear medicine*, 22:351–355, 1995.

[28] H. Li and O. Chutatape. Automatic location of optic disc in retinal images. *International Conference on Image Processing*, 2001.

[29] D. Lloret, J. Serrat, A. Lopez, A. Soler, and J. Villanueva. Retinal image registration using creases as anatomical landmarks. *Proceedings of IEEE International Conference on Image Processing*, 3:203–207, 2000.

[30] A. Lopez, D. Lloret, J. Serrat, and J. Villaneuva. Multilocal creaseness based on the level set extrinsic curvature. *Computer Vision and Image Understanding*, 77, 2000.

[31] F. Maes, A. Collignon, D. Vandermeulen, G. marchal, and P. Suetens. Multimodality image registration by maximization of mutual information. *IEEE Transaction on Medical Imaging*, 16:187–198, 1997.

[32] M. E. Martinez-Perez, A. D. Hughes, A. V. Stanton, S. A. Thom, N. chapman, A. A. Bharath, and K. H. Parker. Retinal vascular tree morphology: A semi-automatic quantifcation. *IEEE Transactions on Biomedical Engineering*, 49:912–917, 2002.

[33] G. K. Matsopoulos, N. A. Mouravliansky, K. K. Delibasis, and K. S. Nikita. Automatic retinal image registration scheme using global optimization techniques. *IEEE Transaction on Information Technology on Biomedicine*, 3:47–60, 1999.

[34] B. J. McParland and J. C. Kumaradas. Digital portal image registration by sequential anatomical matchpoint and image correlations for real-time continuous field alignment verfication. *Medical physics*, 22:1063–1075, 1995.

[35] F. Mendels, C. Heneghan, P. Harper, R. B. Reilly, and J.-P. Thiran. Extraction of the optic disc boundary in digital fundus images. *First Joint BMES/EMBS Conference*

Serving Humanity, Advancing Technology, 1999.

[36] F. Mendels, C. Heneghan, and J.-P. Thiran. Identification of the optic disc boundary in retinal images using active contours. *Irish Machine Vision and Image Processing Conference*, 1999.

[37] A. Mendonca, J. Campilho, and A. Nunes. A new similarity criterion for retinal image registration. *Proceedings of IEEE International conference on Image Processing*, pages 696–700, 1994.

[38] C. R. Meyer, G. S. Leichtman, J. A. Brunberg, R. L. Wahl, and L. E. Quint. Simultaneous usage of homologous points, lines, and planes for optimal, 3-d, linear registration of multimodality imaging data. *IEEE Transactions on medical imaging*, 14:1–11, 1995.

[39] D. T. Morris and C. Donnison. Identifying the neuro-retinal rim boundary using dynamic contours. *Image and Vision Computing 17*, 1999.

[40] N. Mourvliansky, G. Matsopoulos, K. Delibasis, and K. Nikita. Automatic retinal registration using global optimization techniques. *20th IEEE International Conference on Engineering in Medicine and Biology*, 2, 1998.

[41] J. Noack and D. Sutton. An algorithm for the fast registration of image sequences obtained with a scanning laser ophthalmoscope. *Physics in Medicine and Biology*, 39:907–915, 1994.

[42] P. Pallawala, W. Hsu, M. L. Lee, and K. G. A. Eong. Automated optic disc localization and contour detection using ellipse fitting and wavelet transform. *8th European Conference on Computer Vision (ECCV)*, 2004.

[43] E. Peli, R. A. Augliere, and G. T. Timberlake. Feature-based registration of retinal images. *IEEE Transactions on Medical Imaging*, 6:272–278, 1987.

[44] G. P. Penny, J. Weese, J. A. Little, P. Desmedt, D. L. Hill, and D. J. Hawkes. A comparison of similarity measures for used in 2-d-3-d medical image registration. *IEEE Transactions on Medical Imaging*, 17:586–594, 1998.

[45] A. Pinz, S. Bernogger, P. Datlinger, and A. Kruger. Mapping the human retina. *IEEE Transactions on Medical Imaging*, 17:606–619, 1998.

[46] W. K. Pratt. Digital image processing, 2nd edition. *New York: Wiley*, 1991.

[47] F. K. H. Quek and C. Kirbas. Vessel extraction in medical images by wave-propagation and traceback. *IEEE Transactions on Biomedical Engineering*, 49:117–131, 2002.

[48] N. Ritter, R. Owens, J. Cooper, R. H. Eikelboom, and P. P. V. Saarloos. Registration of stereo and temporal images of the retina. *IEEE Transactions on Medical Imaging*, 18:404–418, 1999.

[49] G. K. Rohde, A. Aldroubi, and B. M. Dawant. The adaptive bases algorithm for intensity-based nonrigid image registration. *IEEE Transactions on Medical Imaging*, 22:1470–1479, 2003.

[50] S. Sandor and R. Leahy. Matching deformable atlas models to preprocessed magnetic resonance brain images. *International conference on image processing*, pages 686–690, 1994.

[51] A. Savi, M. C. Gilardi, G. Rizzo, M. Pepi, C. Landoni, C. Rossetti, G. Lucignani, A. Bartorelli, and F. Fazio. Spatial registration of echocardiographic and positron emission tomographic heart studies. *European journal of nuclear medicine*, 22:243–247, 1995.

[52] D. A. Simon, R. V. OToole, M. Blackwell, F. Morgan, A. M. DiGioia, and T. Kanade. Accuracy validation in imageguided orthopaedic surgery. *Medical robotics and computer assisted surgery*, 19:185–192, 1995.

[53] D. E. Singer, D. M. Nathan, H. A. Fogel, and A. P. Schachar. Screening for diabetic retinopathy. *Annual International Medicine*, 116:660–671, 1992.

[54] C. Sinthanayothin, J. F. Boyce, H. L. Cook, and T. H. Williamson. Automated localization of optic disc, fovea and retinal blood vessels from digital color fundus images. *British Journal of Ophthalmology*, 1999.

[55] M. Soltys, D. V. Beard, V. Carrasco, S. Mukherji, and J. Rosenman. Fusion: a tool for registration and visualization of multiple modality 3d medical data. *Medical imaging: image processing*, 2434:74–80, 1995.

[56] S. J. Stapleton, C. B. Caldwell, L. E. Ehrlich, C. L. Leonhardt, S. E. Black, and M. J. Yaffe. Effects on non-linear flow and spatial orientation on technetium-99m hexamethylpropylene amin oxime single-photon emission tomography. *European journal of nuclear medicine*, 22:1009–1016, 1995.

[57] C. V. Stewart, C. L. Tsai, and B. Roysam. The dual-bootstrap iterative closest point algorithm with application to retinal image registration. *IEEE Transactions on Medical Imaging*, 22:1379–1394, 2003.

[58] J. Thirion. New feature points based on geometric invariants for 3d image registration. *International journal of computer vision*, 18:127–137, 1996.

[59] T. G. Turkington, J. M. Hoffman, R. J. Jaszczak, J. R. MacFall, C. C. Harris, C. D. Kilts, C. A. Pelizzari, and R. E. Coleman. Accuracy of surface fit registration for pet and mr brain images using full and incomplete brain surfaces. *Journal of computer assisted tomography*, 19:117–124, 1995.

[60] M. Uenohara and T. Kanade. Vision-based object registration for real-time image overlay. *Computer vision, virtual reality, and robotics in medicine*, pages 13–22, 1995.

[61] D. Vandermeulen, A. Collignon, J. Michiels, H. Bosmans, P. Suetens, G. Marchal, G. Timmens, P. van den Elsen, M. Viergever, H. Ehricke, D. Hentschel, and R. Graumann. Multi-modality image registration within covira. *Medical imaging: analysis of multimodality 2D/3D images*, 19:29–42, 1995.

[62] P. Vassal, J. Troccaz, N. Laieb, P. Cinquin, M. Bolla, and E. Berland. Introducing computer vision sensors in radiotherapy for accurate dose selivery. *Medical robotics and computer assisted surgery*, pages 16–23, 1995.

[63] P. Viola and W. M. W. III. Alignment by maximization of mutual information. *International Journal of Computer Vision*, 24:137–154, 1997.

[64] A. R. Wade and F. W. Fitzke. A fast, robust pattern recognition system for low light level image registration and its application to retinal imaging. *Optics Express*, 3:190–197, 1998.

[65] T. Y. Wong, M. D. Knudtson, R. Klein, B. E. K. Klein, and L. D. Hubbard. A prospective cohort study of retinal arteriolar narrowing and mortality. *American Journal of Epidemiol*, 159:819–825, 2004.

[66] F. Zana and J. C. Klein. A multimodal registration algorithm of eye fundus images using vessels detection and hough transform. *IEEE Transactions on Medical Imaging*, 18:419–428, 1999.

[67] F. Zana and J. C. Klein. Segmentation of vessel-like patterns using mathematical morphology and curvature evaluation. *IEEE Transactions on Image Processing*, 10:1010–1019, 2001.

[68] L. Zhou, M. Rzeszotarski, L. Singerman, and J. Chokreff. The detection and quantification of retinopathy using digital angiograms. *IEEE Transactions on Medical Image*, 13:619–626, 1994.

[69] I. G. Zubal, S. S. Spencer, J. S. K. Imam, E. O. Smith, G. Wisniewski, and P. B. Hoffer. Difference images calculated from ictal and interictal technetium-99m-hmpao spect scans of epilepsy. *Journal of nuclear medicine*, 36:684–689, 1995.